10 ADVANCED PLASTICITY MODELS

THIS chapter is devoted to more advanced plasticity models. Recall that, in Chapters 7–9, all examples of numerical implementation of plasticity models have been limited to basic theories. Here, we move one step further and apply the same underlying concepts to more advanced models. Sections 10.1 and 10.2 describe, respectively, the treatment of a modified Cam-Clay model and a capped Drucker–Prager model – both mainly applicable to the description of geomaterials. Section 10.3 introduces the modelling of anisotropic plasticity. In this context, the Hill model (Hill, 1950), a model based on the Hoffman anisotropic criterion (Hoffman, 1967) – here referred to as the Hoffman model – and the Barlat–Lian model for sheet metals (Barlat and Lian, 1989) are discussed in detail, together with the computational treatment of the Hoffman and Barlat–Lian models with isotropic strain hardening.

The new theoretical concepts introduced in this chapter are, essentially, the modelling of plastic compaction – a phenomenon of particular relevance in the behaviour of geomaterials – and the modelling of plastic anisotropy. Note, however, that the computational implementation of elastoplastic models possessing such new features reduces to mere specialisations of the general framework discussed in the preceding chapters.

10.1. A modified Cam-Clay model for soils

The modified Cam-Clay model was originally proposed by Roscoe and Burland (1968) to model the plastic behaviour of soils. Models of this type are frequently used in the finite element modelling of soil mechanics problems. These models are characterised by plastic compressibility, hardening (softening) associated with compressive (dilatant) plastic flow and a possibly nonlinear elasticity law to model the hydrostatic pressure/volumetric elastic strain relation (refer, for instance, to Naylor *et al.* 1981, and Muir Wood 1990). In many cases, when dealing with soil consolidation problems, Cam-Clay-type models can be used within a multiphase environment with coupling between solid behaviour and flow through porous media. Such problems are outside the scope of this book and we shall describe in this section a version of the modified Cam-Clay plasticity model featuring a linear elasticity law and a standard volumetric plastic strain-dependent isotropic hardening rule. In soil mechanics applications, the use of a linear elastic law can be justified whenever the considered range of hydrostatic pressures is sufficiently narrow.

Computational Methods for Plasticity: Theory and Applications EA de Souza Neto, D Perić and DRJ Owen
 ISBN: 978-0-470-69452-7

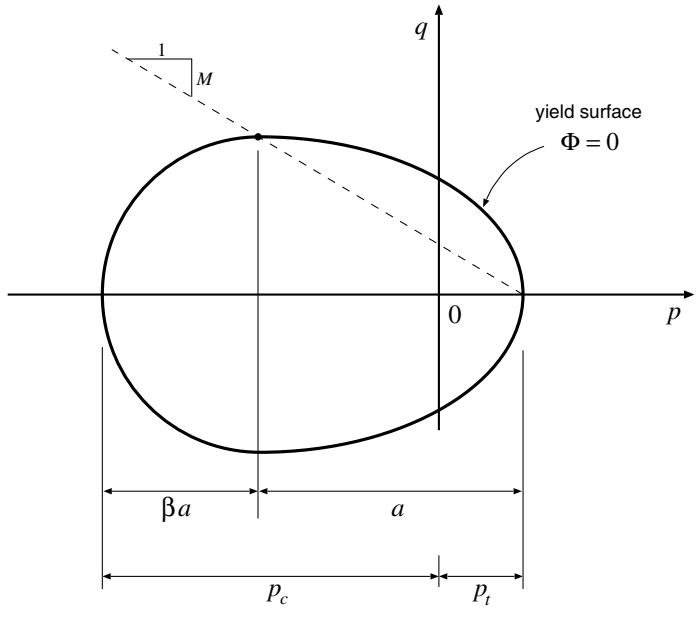

Figure 10.1. Modified Cam-Clay model. Yield surface.

10.1.1. THE MODEL

Let p and q denote, respectively, the hydrostatic stress and the von Mises effective stress. The elastic domain of the modified Cam-Clay model is delimited by an elliptic yield surface in the p–q space. Here, we will focus on a version of the modified Cam-Clay model whose yield surface (refer to Figure 10.1) is defined by a yield function of the form

$$\Phi(\boldsymbol{\sigma}, a) = \frac{1}{b^2}\left[p(\boldsymbol{\sigma}) - p_t + a\right]^2 + \left[\frac{q(\boldsymbol{\sigma})}{M}\right]^2 - a^2, \tag{10.1}$$

where the constant M is the ratio between the two radii of the Cam-Clay ellipse, a is the radius of the ellipse along the pressure axis and p_t is the tensile yield hydrostatic stress. The parameter b takes the values

$$b = \begin{cases} 1 & \text{if } p \geq p_t - a \\ \beta & \text{if } p < p_t - a, \end{cases} \tag{10.2}$$

where β is a material constant. This parameter modifies the radius of the second half of the ellipse on the compressive side of the hydrostatic axis. If $\beta = 1$, the yield locus becomes an ellipse with radii a and Ma, respectively, along directions p and q. Note that, for any $\beta > 0$, the two horizontal halves of the surface intersect in a smooth fashion at $(p, q) = (p_t - a, Ma)$. The dashed line in Figure 10.1 is named the *critical state line*. The parameter M is the slope of the critical state line. The portion of the p–q plane on the right of the intersection between the critical state line and the Cam-Clay ellipse is named the *supercritical* region and the portion on its left is the *subcritical* region.

Flow rule

The plastic flow equation can be defined by postulating associativity, which gives

$$\dot{\boldsymbol{\varepsilon}}^p = \dot{\gamma}\,\frac{\partial \Phi}{\partial \boldsymbol{\sigma}} = \dot{\gamma}\,\boldsymbol{N} = \dot{\gamma}\,(\boldsymbol{N}_{\mathrm{d}} + N_{\mathrm{v}}\boldsymbol{I}\,), \tag{10.3}$$

where we have conveniently split the flow vector, $\boldsymbol{N} = \partial\Phi/\partial\boldsymbol{\sigma}$, into deviatoric and volumetric components, respectively denoted $\boldsymbol{N}_{\mathrm{d}}$ and N_{v}:

$$\boldsymbol{N}_{\mathrm{d}} = \frac{3}{M^2}\,\boldsymbol{s}; \quad N_{\mathrm{v}} = \frac{2}{b^2}\,(p - p_t + a). \tag{10.4}$$

The deviatoric and volumetric plastic strain rates then read

$$\dot{\boldsymbol{\varepsilon}}^p_{\mathrm{d}} = \dot{\gamma}\,\boldsymbol{N}_{\mathrm{d}}; \quad \dot{\varepsilon}^p_{\mathrm{v}} = \dot{\gamma}\,N_{\mathrm{v}}. \tag{10.5}$$

The plastic flow defined by the above associative rule is compressive[†] ($\dot{\varepsilon}^p_{\mathrm{v}} < 0$) if $p < p_t - a$ (subcritical states), dilatant ($\dot{\varepsilon}^p_{\mathrm{v}} > 0$) if $p > p_t - a$ (supercritical states) and isochoric ($\dot{\varepsilon}^p_{\mathrm{v}} = 0$) at $p = p_t - a$ (critical state).

Hardening law

A simple way of incorporating hardening into the model consists in letting the yield surface parameter a be a function of a hardening internal variable,[‡] α. For many plastically compressible materials, and for soils in particular, the state of hardening is largely dependent upon the volumetric plastic strain (or plastic compaction),

$$\varepsilon^p_{\mathrm{v}} \equiv \mathrm{tr}[\boldsymbol{\varepsilon}^p]. \tag{10.6}$$

Because in actual applications, soils will be predominantly subjected to *compressive* strains, the hardening variable, α, will be chosen as the *compressive-positive* volumetric plastic strain:

$$\alpha \equiv -\varepsilon^p_{\mathrm{v}} \tag{10.7}$$

and the hardening behaviour will be defined by means of the experimentally determined hardening function

$$a = a(\alpha). \tag{10.8}$$

Equivalently, in terms of the *compressive yield pressure* (or *compaction pressure*), p_c (also assumed compressive-positive) hardening can be defined by

$$p_c(\alpha) \equiv (1 + \beta)\,a(\alpha) - p_t. \tag{10.9}$$

Under this assumption, the evolution of the volumetric plastic strain will change the size of the modified Cam-Clay yield surface while maintaining its shape. Hardening in this case is characterised by a change in compressive yield pressure, having the intersection of the yield surface with the p-axis at $p = p_t$ (the tensile yield pressure) fixed.

[†]Consistently with the continuum mechanics sign convention adopted throughout this book, compressive volumetric strains and hydrostatic pressures have a negative sign here. It should be noted that the opposite sign convention is commonly adopted in soil mechanics texts, where compressive volumetric strains and hydrostatic pressures are assumed positive.

[‡]In a more general setting, other yield surface parameters such as M or β could also be functions of hardening variables.

Remark 10.1 (Hardening behaviour). The hardening function $a(\alpha)$ (or $p_c(\alpha)$) is usually expected to be monotonically increasing in its argument, that is, a increases with increasing plastic compression. In this case, following the comments on the volumetric plastic strain rate made immediately after expression (10.5), hardening (expansion of the elastic domain) occurs only in the subcritical region, i.e. under hydrostatic pressures $p < p_t - a$. For pressures $p > p_t - a$ (supercritical states) plastic flow will cause *softening* (contraction of the elastic domain) and at $p = p_t - a$ (the critical state) the model behaves as perfectly plastic (fixed yield surface).

10.1.2. COMPUTATIONAL IMPLEMENTATION

Here we shall adopt a linear elasticity law to model the reversible behaviour of the modified Cam-Clay model. We remark, however, that it is sometimes convenient to adopt nonlinear elasticity laws with models of this type. The implementation of Cam-Clay-type models with nonlinear elastic laws is described, for instance, by Simo and Meschke (1993) and Owen *et al.* (1998).

The return-mapping algorithm

The elastic trial state computation follows the usual format:

$$\boldsymbol{s}^{\mathrm{trial}} = 2G\,\boldsymbol{\varepsilon}_{\mathrm{d}}^{e\,\mathrm{trial}}; \quad p^{\mathrm{trial}} = K\,\varepsilon_{\mathrm{v}}^{e\,\mathrm{trial}}. \tag{10.10}$$

The return-mapping algorithm is derived as follows. Firstly, by observing the deviatoric/volumetric split (10.4) of the plastic flow and the elastic relations, the following stress update equations consistent with the implicit discretisation of the plastic flow rule are obtained:

$$\begin{cases} \boldsymbol{s}_{n+1} = \boldsymbol{s}^{\mathrm{trial}} - 2G\Delta\gamma\,\dfrac{3}{M^2}\,\boldsymbol{s}_{n+1}; \\ \\ p_{n+1} = p^{\mathrm{trial}} - K\Delta\gamma\,\dfrac{2}{b^2}[p_{n+1} - p_t + a(\alpha_{n+1})], \end{cases} \tag{10.11}$$

where the updated hardening variable is given by the equation

$$\alpha_{\,n+1} = \alpha_{\,n} - \Delta\gamma\,\frac{2}{b^2}[p_{n+1} - p_t + a(\alpha_{n+1})]. \tag{10.12}$$

In addition, the discrete consistency equation here reads

$$\Phi_{n+1} = \frac{1}{b^2}\,[p_{n+1} - p_t + a(\alpha_{n+1})]^2 + \left(\frac{q_{n+1}}{M}\right)^2 - [a(\alpha_{n+1})]^2 = 0, \tag{10.13}$$

where q_{n+1} is the von Mises effective stress associated with $\boldsymbol{s}_{n+1}$.

Particularisation of the general return-mapping equations (7.25) (page 196) for the present model results in the system of equations comprising (10.11)–(10.13), having α_{n+1}, p_{n+1}, the linearly independent components of $\boldsymbol{s}_{n+1}$ and the incremental plastic multiplier, $\Delta\gamma$, as the unknowns.

Reduced equation system

In order to obtain an equivalent reduced system of equations for the return mapping, we start by noting that $(10.11)_1$ implies that for a given $\boldsymbol{s}^{\text{trial}}$ the updated stress deviator, $\boldsymbol{s}_{n+1}$, is a function of $\Delta\gamma$ only; that is, after a simple rearrangement in $(10.11)_1$ we obtain

$$\boldsymbol{s}_{n+1} = \boldsymbol{s}(\Delta\gamma) \equiv \frac{M^2}{M^2 + 6G\,\Delta\gamma}\,\boldsymbol{s}^{\text{trial}}, \tag{10.14}$$

and, similarly, for q_{n+1},

$$q_{n+1} = q(\Delta\gamma) \equiv \frac{M^2}{M^2 + 6G\,\Delta\gamma}\,q^{\text{trial}}. \tag{10.15}$$

In addition, by combining $(10.11)_2$ and (10.12) we can write

$$p_{n+1} = p(\alpha_{n+1}) \equiv p^{\text{trial}} + K\,(\alpha_{n+1} - \alpha_n). \tag{10.16}$$

Finally, the substitution of (10.15) and (10.16) in (10.12) and (10.13) leads to the following reduced system of two scalar equations with unknowns $\Delta\gamma$ and α_{n+1}:

$$\left\{\begin{array}{c} R_1 \\ \\ R_2 \end{array}\right\} \equiv \left\{\begin{array}{l} \dfrac{1}{b^2}\,[p(\alpha) - p_t + a(\alpha)]^2 + \left[\dfrac{q(\Delta\gamma)}{M}\right]^2 - [a(\alpha)]^2 \\ \\ \alpha - \alpha_{\,n} + \Delta\gamma\,\dfrac{2}{b^2}[p(\alpha) - p_t + a(\alpha)] \end{array}\right\} = \left\{\begin{array}{c} 0 \\ \\ 0 \end{array}\right\}, \tag{10.17}$$

where the subscript $n+1$ of α_{n+1} has been omitted for notational convenience. Once the solution to the above return-mapping equations is obtained, the stress-updating procedure is completed with the computation of $\boldsymbol{s}_{n+1}$ by means of (10.14), followed by the calculation of the updated stress tensor through the standard relation

$$\boldsymbol{\sigma}_{n+1} = \boldsymbol{s}_{n+1} + p_{n+1}\,\boldsymbol{I}. \tag{10.18}$$

It is worth commenting here that system (10.17) could in principle be further reduced to a single scalar equation having α_{n+1} as the only unknown by trivially solving the second equation of (10.17) for $\Delta\gamma$:

$$\Delta\gamma = \Delta\gamma(\alpha_{n+1}) \equiv \frac{b^2(\alpha_n - \alpha_{n+1})}{2[p(\alpha_{n+1}) - p_t + a(\alpha_{n+1})]}, \tag{10.19}$$

and then replacing this result into the first equation. It should be noted, however, that the above expression cannot be used in practice at $p = p_t - a$.

Newton–Raphson solution

The solution of (10.17) can be undertaken as usual by the Newton–Raphson algorithm. For completeness, an explicit expression for the linear system to be solved for the iterative

corrections $\delta\Delta\gamma^{(k)}$ and $\delta\alpha^{(k)}$ at the typical k^{th} Newton iteration is shown below:

$$\begin{bmatrix} \dfrac{-12\,G}{M^2+6G\Delta\gamma}\left(\dfrac{q}{M}\right)^2 & \dfrac{2\bar{p}}{b^2}(K+H)-2aH \\ \dfrac{2\bar{p}}{b^2} & 1+\dfrac{2\Delta\gamma}{b^2}(K+H) \end{bmatrix} \begin{Bmatrix} \delta\Delta\gamma^{(k)} \\ \delta\alpha^{(k)} \end{Bmatrix} = \begin{Bmatrix} R_1^{(k-1)} \\ R_2^{(k-1)} \end{Bmatrix}, \tag{10.20}$$

where H is the hardening modulus (the slope of the hardening curve):

$$H = H(\alpha) \equiv \frac{\mathrm{d}a}{\mathrm{d}\alpha}, \tag{10.21}$$

the scalar $\bar{p}$ is defined as

$$\bar{p} = \bar{p}(\alpha) \equiv p(\alpha) - p_t + a(\alpha), \tag{10.22}$$

and all terms of the derivative matrix on the right-hand side are evaluated at $(\Delta\gamma, \alpha) = (\Delta\gamma^{(k-1)}, \alpha_{n+1}^{(k-1)})$.

The elastoplastic consistent tangent

To derive the elastoplastic consistent tangent operator for the above implementation of the modified Cam-Clay model, we resort to the general procedure of Section 7.4.4 (from page 238), which was also applied in Section 7.4.5 (page 240) as an alternative to the derivation of the elastoplastic consistent tangent for the implicit integration of the von Mises model. Accordingly, we start by differentiating the full system of return-mapping equations which, in the present case, comprises (10.11)–(10.13) together with the trivial update formula (10.18). The differentiation, in which the elastic trial strain tensor is also treated as a variable, yields the tangential relationship

$$\begin{bmatrix} [\mathsf{D}^e]^{-1}+\Delta\gamma\,\partial\boldsymbol{N}/\partial\boldsymbol{\sigma} & 0 & \boldsymbol{N} \\ \Delta\gamma\,\partial N_{\mathrm{v}}/\partial\boldsymbol{\sigma} & 1+\dfrac{2H\Delta\gamma}{b^2} & N_{\mathrm{v}} \\ \boldsymbol{N} & \partial\Phi/\partial\alpha & 0 \end{bmatrix} \begin{Bmatrix} \mathrm{d}\boldsymbol{\sigma}_{n+1} \\ \mathrm{d}\alpha_{n+1} \\ \mathrm{d}\Delta\gamma \end{Bmatrix} = \begin{Bmatrix} \mathrm{d}\boldsymbol{\varepsilon}^{e\,\mathrm{trial}} \\ 0 \\ 0 \end{Bmatrix}, \tag{10.23}$$

where, following the deviatoric/volumetric split of (10.3), we write

$$\frac{\partial\boldsymbol{N}}{\partial\boldsymbol{\sigma}} = \frac{\partial\boldsymbol{N}_{\mathrm{d}}}{\partial\boldsymbol{\sigma}} + \boldsymbol{I}\otimes\frac{\partial N_{\mathrm{v}}}{\partial\boldsymbol{\sigma}} \tag{10.24}$$

with

$$\frac{\partial\boldsymbol{N}_{\mathrm{d}}}{\partial\boldsymbol{\sigma}} = \frac{3}{M^2}\,\mathsf{I}_{\mathrm{d}}; \quad \frac{\partial N_{\mathrm{v}}}{\partial\boldsymbol{\sigma}} = \frac{2}{3b^2}\,\boldsymbol{I}. \tag{10.25}$$

In addition, from (10.13) we obtain

$$\frac{\partial\Phi}{\partial\alpha} = \frac{2}{b^2}\,(p-p_t+a)H - 2aH = (N_{\mathrm{v}}-2a)H. \tag{10.26}$$

Here we should note that tangential relation (10.23) has a similar format to that of (7.141) which was obtained for the implicit implementation of the isotropically hardening von Mises

model. Accordingly, its inversion follows completely analogous steps to those leading to (7.148) and yields the following formula for the elastoplastic consistent tangent operator:

$$\begin{aligned}\mathsf{D}^{ep} &\equiv \frac{\partial \boldsymbol{\sigma}_{n+1}}{\partial \boldsymbol{\varepsilon}^{e\,\mathrm{trial}}} \\ &= \mathsf{P} - \frac{1}{\tilde{\boldsymbol{N}} : \mathsf{P} : \boldsymbol{N} + (N_{\mathrm{v}} - 2a) N_{\mathrm{v}} H} \, (\mathsf{P} : \boldsymbol{N}) \otimes (\mathsf{P} : \tilde{\boldsymbol{N}}),\end{aligned} \tag{10.27}$$

where

$$\mathsf{P} \equiv \left(\mathsf{I}_S + \Delta\gamma \, \mathsf{D}^e : \frac{\partial \boldsymbol{N}}{\partial \boldsymbol{\sigma}} \right)^{-1} : \mathsf{D}^e \tag{10.28}$$

with flow vector derivative given by (10.24), and

$$\begin{aligned}\tilde{\boldsymbol{N}} &\equiv -\Delta\gamma (N_{\mathrm{v}} - 2a) H \, \frac{\partial N_{\mathrm{v}}}{\partial \boldsymbol{\sigma}} + \left(1 + \frac{2H\Delta\gamma}{b^2} \right) \boldsymbol{N} \\ &= \frac{-2\Delta\gamma (N_{\mathrm{v}} - 2a) H}{3b^2} \, \boldsymbol{I} + \left(1 + \frac{2H\Delta\gamma}{b^2} \right) \boldsymbol{N}.\end{aligned} \tag{10.29}$$

Since in general $\tilde{\boldsymbol{N}} \neq \boldsymbol{N}$, the elastoplastic tangent operator (10.27) is generally *unsymmetric*. Its non-symmetry is a consequence of the non-associativity of the adopted hardening law. The reader is referred to the discussion at the beginning of Section 7.4.6, from page 243. Also note that in the absence of hardening, that is, if $H = 0$, $\tilde{\boldsymbol{N}}$ coincides with $\boldsymbol{N}$ and symmetry is recovered.

10.2. A capped Drucker–Prager model for geomaterials

The *standard* Drucker–Prager model has been described in detail in Chapter 6 and its computational implementation has been addressed in Section 8.3 (from page 324). For that model (as well as for the Mohr–Coulomb model), the application of an arbitrary compressive hydrostatic pressure alone does not cause plastic flow. Plastic flow under compressive hydrostatic pressure may only be triggered with the superposition of shearing stresses. For many geomaterials, however, compressive plastic flow (compaction) under (possibly pure) compressive hydrostatic stresses can be an important feature of the overall behaviour. In circumstances where plastic compaction is relevant, the standard Drucker–Prager or Mohr–Coulomb plasticity models are not able to capture the actual material behaviour.

The modified Cam-Clay model discussed in the previous section already incorporates the possibility of plastic compaction. Another alternative for modelling such a phenomenon consists in bounding the standard Drucker–Prager yield surface with a *cap* on the compressive side of the hydrostatic axis. A particularly simple choice is the adoption of an *elliptical* cap as the compressive bounding surface. The p–q plane representation of the yield surface so obtained is illustrated in Figure 10.2. The equations of the resulting multisurface (two-surface) model, followed by an outline of its numerical treatment, is presented below. The implementation of a Cap-type model similar to that described here is presented by Simo *et al.* (1988a).

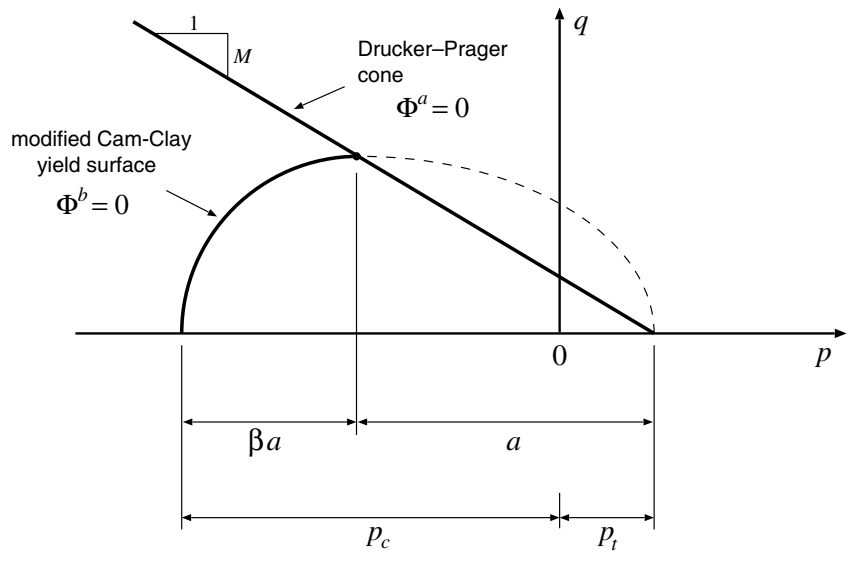

Figure 10.2. Capped Drucker–Prager model. Yield surface.

10.2.1. CAPPED DRUCKER–PRAGER MODEL

The yield functions of the model are

$$\begin{aligned} \Phi^a(\boldsymbol{\sigma}) &\equiv \sqrt{J_2(\boldsymbol{s}(\boldsymbol{\sigma}))} + \eta\,[p(\boldsymbol{\sigma}) - p_t]; \\ \Phi^b(\boldsymbol{\sigma}, a) &= \frac{1}{\beta^2}\,[p(\boldsymbol{\sigma}) - p_t + a]^2 + \left[\frac{q(\boldsymbol{\sigma})}{M}\right]^2 - a^2, \end{aligned} \tag{10.30}$$

where Φ^a is an equivalent representation of the Drucker–Prager yield function obtained from its original expression (6.121) (page 167) by using the trivial relation

$$c = \frac{\eta}{\xi}\, p_t, \tag{10.31}$$

and $\Phi^b = 0$ defines the elliptical cap – the modified Cam-Clay yield surface for subcritical states discussed in the previous section of this chapter. In $(10.30)_1$,

$$\eta = \sqrt{2/3}\, M. \tag{10.32}$$

For a fixed a, the set of plastically admissible stress states is defined by

$$\mathscr{A} = \{\boldsymbol{\sigma} \mid \Phi^a(\boldsymbol{\sigma}) \leq 0,\ \Phi^b(\boldsymbol{\sigma}, a) \leq 0\}. \tag{10.33}$$

Plastic flow rule

On the cone, the standard generally non-associative Drucker–Prager flow rule is adopted. On the smooth part of the cone, the plastic strain rate equation is given by (6.157)

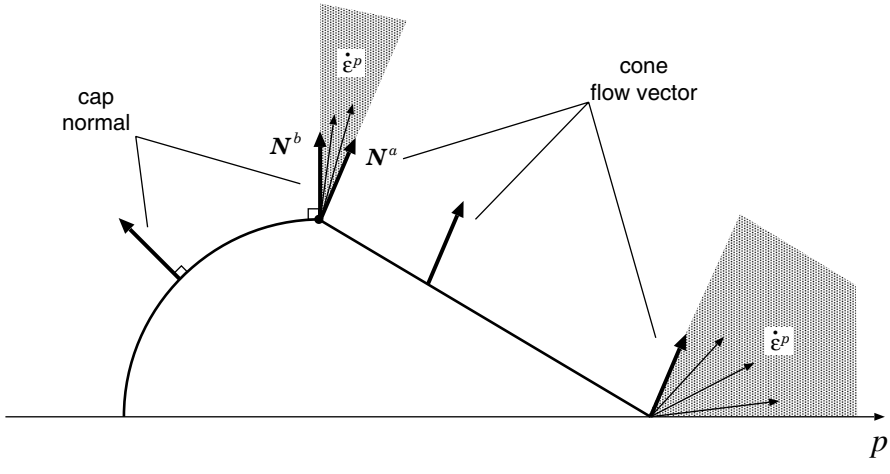

Figure 10.3. Capped Drucker–Prager model. Flow vectors.

(page 176), $(6.158)_1$ and (6.166). At the cone apex, the flow vector has deviatoric and volumetric components $(6.160)_1$ and (6.166), respectively. On the cap, the (associative) flow rule is that of the modified Cam-Clay model, given by (10.3) and (10.4).

Following the general representation of associative plastic flow rules for multisurface plasticity models given by (6.73) (page 156), (6.77) and (6.78), the plastic strain rate at the intersection between the Drucker–Prager cone and the elliptical cap reads

$$\dot{\boldsymbol{\varepsilon}}^p = \dot{\gamma}^a \, \boldsymbol{N}^a + \dot{\gamma}^b \, \boldsymbol{N}^b, \tag{10.34}$$

where $\boldsymbol{N}^a$ and $\boldsymbol{N}^b$ are, respectively, the non-associative Drucker–Prager flow vector at the smooth portion of the cone and the associative modified Cam-Clay flow vector referred to above. The flow vector $\boldsymbol{N}^a$ has the standard form

$$\boldsymbol{N}^a = \frac{1}{2\sqrt{J_2(\boldsymbol{s})}} \, \boldsymbol{s} + \frac{\bar{\eta}}{3} \boldsymbol{I}. \tag{10.35}$$

At the cap/cone intersection, where $p = p_t - a$, the normal to the cap with general expression (10.4) is a deviatoric tensor:

$$\boldsymbol{N}^b = \boldsymbol{N}^b_{\mathrm{d}} = \frac{3}{M^2} \, \boldsymbol{s}. \tag{10.36}$$

A general p-q plane illustration of the plastic flow directions for the resulting model is given in Figure 10.3.

Hardening

As for the previously discussed modified Cam-Clay model (refer to expressions (10.9) and (10.8)) isotropic strain hardening is incorporated by letting the compaction pressure p_c (or, equivalently, the yield surface parameter a) be a function of the compressive-positive

volumetric plastic strain, α, defined in (10.7). The Drucker–Prager cone remains fixed and is independent of the hardening variable.

As p_c increases (decreases), the cap moves in the compression (tensile) direction along the hydrostatic line, expanding (shrinking) the elastic domain.

10.2.2. THE IMPLICIT INTEGRATION ALGORITHM

The integration algorithm for the present model is a combination of the elastic predictor/return-mapping schemes derived in Sections 8.3.1 (from page 325) and 10.1.2 for the Drucker–Prager and modified Cam-Clay models, respectively. The two-surface model admits four possible return mappings:

1. return to the smooth portion of the Drucker–Prager cone;
2. return to the cone apex;
3. return to the elliptic cap;
4. return to the cone/cap intersection.

The return mappings to the smooth portion and apex of the Drucker–Prager cone are a particular instance of the procedure described in Section 8.3 (from page 324), with the added simplicity of perfect plasticity. In this case (refer to Remark 8.4, page 327), the return-mapping equations can be solved in closed form. The return mapping to the cap surface, in turn, is that of the modified Cam-Clay model discussed in Section 10.1.2.

The plastic corrector algorithm for the cone/cap intersection is a two-vector return mapping where the incremental plastic strain is given by the discrete form of (10.34)–(10.36):

$$\Delta\boldsymbol{\varepsilon}^p = \Delta\gamma^a\, \boldsymbol{N}^a + \Delta\gamma^b\, \boldsymbol{N}^b. \tag{10.37}$$

Its volumetric component reads

$$\varepsilon_{\mathrm{v}}^p = \bar{\eta}\, \Delta\gamma^a. \tag{10.38}$$

so that the update formula for the hardening internal variable at the cone/cap intersection is given by

$$\alpha_{n+1} = \alpha_n - \bar{\eta}\, \Delta\gamma^a. \tag{10.39}$$

The return-mapping equation for the cone/cap intersection is derived by introducing (10.37) into the general stress update formula

$$\begin{aligned} \boldsymbol{s}_{n+1} &= \boldsymbol{s}_{n+1}^{\mathrm{trial}} - 2G\Delta\boldsymbol{\varepsilon}_{\mathrm{d}}^p, \\ p_{n+1} &= p_{n+1}^{\mathrm{trial}} - K\Delta\varepsilon_{\mathrm{v}}^p, \end{aligned} \tag{10.40}$$

and then substituting the resulting expression, together with (10.39) into the cone/cap intersection consistency equation

$$\begin{aligned} \Phi_{n+1}^a &\equiv \sqrt{J_2(\boldsymbol{s}_{n+1})} + \eta[p_{n+1} - p_t] = 0 \\ \Phi_{n+1}^b &\equiv \frac{1}{\beta^2}\,[p_{n+1} - p_t + a(\alpha_{n+1})]^2 + \left[\frac{q(\boldsymbol{s}_{n+1})}{M}\right]^2 - [a(\alpha_{n+1})]^2 = 0. \end{aligned} \tag{10.41}$$

The derivation of the final equations for the unknown multipliers $\Delta\gamma^a$ and $\Delta\gamma^b$ is straightforward and will be left as an exercise for the interested reader.

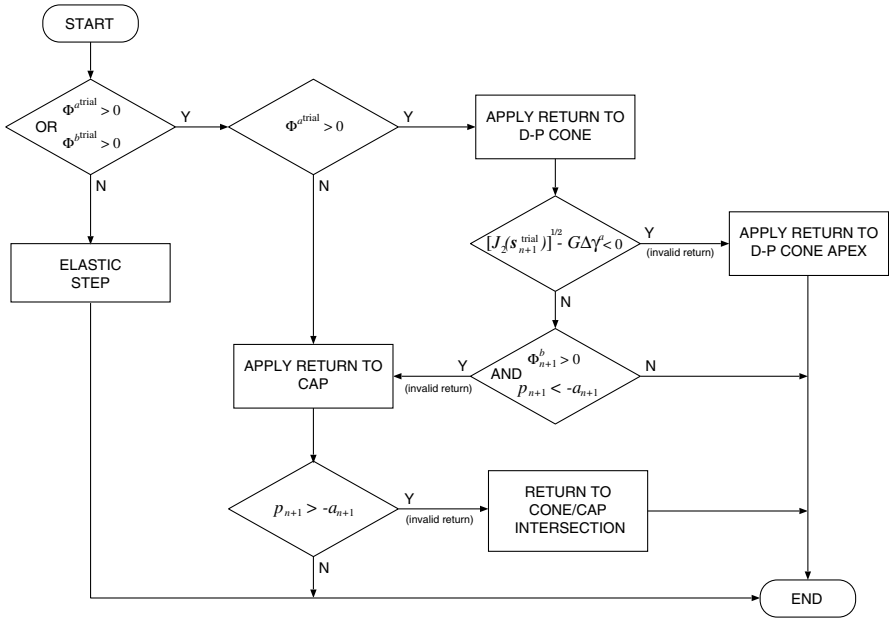

Figure 10.4. Capped Drucker–Prager model. Algorithm for selection of the correct return-mapping procedure.

Selection of the appropriate return mapping

As discussed in detail in Chapter 8, when dealing with multivector implementations of multisurface plasticity models, an appropriate algorithm has to be devised to select, for a given elastic trial state, the return mapping that fully satisfies plastic consistency. The selection algorithm in the present case is an extension of that of the conventional Drucker–Prager model represented in the flowchart of Figure 8.15 (page 330). Its validity can also be established on the basis of geometrical arguments. This will be left as an exercise for the reader. The summary of a possible selection algorithm is shown in the flowchart of Figure 10.4.

10.2.3. THE ELASTOPLASTIC CONSISTENT TANGENT OPERATOR

The elastoplastic consistent tangent will be dependent on the particular return mapping considered, as four distinct return procedures are possible for the present model. The situation here is an extension of that studied in Chapter 8 for the standard Drucker–Prager model. The basic rule for selection of the elastoplastic tangent to be used is the same: the tangent operator must be consistent with the last return-mapping procedure used in the material point (Gauss point of the finite element mesh) considered; that is, if the return to the main Drucker–Prager cone was used in the last stress update for that point, then the current elastoplastic tangent will be consistent with the Drucker–Prager cone return. If the cone–cap intersection was the last return mapping used, then the current tangent will be consistent with the cone–cap intersection return, and so on.

The tangent operator consistent with the Drucker–Prager cone and cone apex return algorithms are those derived in Section 8.3.4 (from page 337) which, for the present model, must be particularised for the perfectly plastic case. Note that, in this case, at the cone apex, we have

$$\mathbf{D}^{ep} = \mathbf{0}. \tag{10.42}$$

For the cap return, the tangent operator is that of (10.27) with $b = \beta$ in (10.29). The derivation of an explicit form for the tangent for the cone/cap intersection return follows an analogous procedure to those of the two-vector return mappings discussed in Chapter 8 and will be left as an exercise for the reader.

10.3. Anisotropic plasticity: the Hill, Hoffman and Barlat–Lian models

The elastoplasticity theories discussed so far in this book have been limited by the assumption of elastoplastic *isotropy*; that is, elastic properties (Young's modulus and Poisson's ratio) as well as plastic properties such as yield stress and hardening behaviour have been assumed independent of material orientation. However, in many circumstances of practical interest, material behaviour is truly *anisotropic* with substantial discrepancy among phenomenological properties observed in different material directions.

An important instance of anisotropic behaviour arises in polycrystalline metals. Such metals are aggregates of single crystals whose individual plastic behaviour is highly anisotropic (physical aspects and the numerical treatment of single crystal plasticity are addressed in Chapter 16). Polycrystalline aggregates with sufficiently random crystal orientation distribution present an effectively isotropic macroscopic behaviour and can be modelled by conventional isotropic plasticity theories. However, when such materials undergo manufacturing processes characterised by extreme straining along preferential directions (rolling is a typical example), the development of texturing (reorientation of crystals according to the direction of straining) results in a final crystallographic arrangement whose macroscopic behaviour is clearly anisotropic. This property is known as *strain-induced* plastic anisotropy and is often present in formed metal components. Another class of materials whose anisotropy can be of particular relevance are composites in general. Many such materials (fibre-reinforced polymers are typical examples) are designed so as to produce optimal strength/performance along predefined directions.

In such cases, the isotropy assumption may lead to a poor representation of the actual behaviour and the formulation and use of appropriate anisotropic plasticity models becomes crucial to ensure reasonable accuracy in finite element predictions. In this section, we address the modelling and computational implementation of anisotropic phenomenological plasticity models. Attention is focused on the orthotropic models proposed by Hill (1948, 1950), Hoffman (1967) and Barlat and Lian (1989).

10.3.1. THE HILL ORTHOTROPIC MODEL

The Hill criterion has been introduced as an orthotropic extension of the standard von Mises criterion in order to model the anisotropy often found in formed steel. With σ_{ij} denoting the stress tensor components on an orthonormal basis $\{\boldsymbol{e}_1, \boldsymbol{e}_2, \boldsymbol{e}_3\}$ whose vectors coincide with the principal axes of plastic orthotropy, the yield function associated with the Hill criterion

can be cast in the following form:

$$\Phi(\boldsymbol{\sigma}, \bar{\sigma}) = F_1 \, (\sigma_{11} - \sigma_{22})^2 + F_2 \, (\sigma_{22} - \sigma_{33})^2 + F_3 \, (\sigma_{33} - \sigma_{11})^2 + F_4 \, \sigma_{12}^2 + F_5 \, \sigma_{23}^2 + F_6 \, \sigma_{13}^2 - \bar{\sigma}^2, \tag{10.43}$$

where $\bar{\sigma}$ is the *relative yield stress* (a non-dimensional scalar) which defines the size (state of hardening) of the yield surface in the six-dimensional space of stress components. The constants F_1, F_2 and F_3 are defined as

$$\begin{aligned} F_1 &= \frac{1}{2}\left(\frac{1}{(\sigma_{11}^0)^2} + \frac{1}{(\sigma_{22}^0)^2} - \frac{1}{(\sigma_{33}^0)^2} \right); \\ F_2 &= \frac{1}{2}\left(\frac{-1}{(\sigma_{11}^0)^2} + \frac{1}{(\sigma_{22}^0)^2} + \frac{1}{(\sigma_{33}^0)^2} \right); \\ F_3 &= \frac{1}{2}\left(\frac{1}{(\sigma_{11}^0)^2} - \frac{1}{(\sigma_{22}^0)^2} + \frac{1}{(\sigma_{33}^0)^2} \right), \end{aligned} \tag{10.44}$$

where σ_{11}^0, σ_{22}^0 and σ_{33}^0 are, respectively, the (generally distinct) uniaxial yield stresses in the directions of $\boldsymbol{e}_1$, $\boldsymbol{e}_2$ and $\boldsymbol{e}_3$ when $\bar{\sigma} = 1$ (here assumed to be the *initial* state of the material). The constants F_4, F_5 and F_6 are defined as

$$F_4 = \frac{1}{(\sigma_{12}^0)^2}; \quad F_5 = \frac{1}{(\sigma_{23}^0)^2}; \quad F_6 = \frac{1}{(\sigma_{13}^0)^2}, \tag{10.45}$$

where σ_{ij}^0 are the three (generally distinct) initial (when $\bar{\sigma} = 1$) yield stresses in pure shear along the corresponding planes orthogonal to the principal directions of orthotropy. For a generic state of hardening (i.e. not necessarily unity $\bar{\sigma}$), the yield stress under a stress state with a single non-zero stress component σ_{ij} is

$$\sigma_{ij}^y = \bar{\sigma} \, \sigma_{ij}^0. \tag{10.46}$$

Indeed, note that under such a stress state it follows from (10.43) that

$$\Phi(\boldsymbol{\sigma}, \bar{\sigma}) = 0 \Longleftrightarrow \sigma_{ij} = \bar{\sigma} \, \sigma_{ij}^0. \tag{10.47}$$

Pressure insensitivity

One important feature of the Hill criterion is the fact that, as for the von Mises and Tresca criteria, it is *pressure insensitive*. This allows us to express its yield function in terms of the components of the stress deviator, $\boldsymbol{s}$, only. By recalling the trivial identities

$$\sigma_{ii} - \sigma_{jj} = s_{ii} - s_{jj}, \tag{10.48}$$

with no summation on repeated indices, and

$$\sigma_{ij} = s_{ij}, \quad \text{for } i \neq j, \tag{10.49}$$

the Hill yield function can be equivalently written as

$$\Phi(\boldsymbol{\sigma}, \bar{\sigma}) = F_1 \, (s_{11} - s_{22})^2 + F_2 \, (s_{22} - s_{33})^2 + F_3 \, (s_{11} - s_{33})^2 + F_4 \, s_{12}^2 + F_5 \, s_{23}^2 + F_6 \, s_{13}^2 - \bar{\sigma}^2. \tag{10.50}$$

Von Mises criterion as a particular case

Another important feature of the Hill criterion is that it recovers the standard von Mises criterion if

$$\sigma_{11}^0 = \sigma_{22}^0 = \sigma_{33}^0 = \sqrt{3}\,\sigma_{12}^0 = \sqrt{3}\,\sigma_{23}^0 = \sqrt{3}\,\sigma_{13}^0. \tag{10.51}$$

To see this, we assume that the above relation holds and set $\sigma_{11}^0 = \sigma_y$ and $\bar{\sigma} = 1$ in (10.50). After a straightforward algebraic manipulation, where we make use of the trivial relation

$$s_{11} + s_{22} + s_{33} = 0, \tag{10.52}$$

we obtain

$$\begin{aligned}\Phi(\boldsymbol{\sigma}, \bar{\sigma}) &= \frac{3}{2\sigma_y^2}[s_{11}^2 + s_{22}^2 + s_{33}^2 + 2(s_{12}^2 + s_{23}^2 + s_{13}^2)] - 1 \\ &= \frac{3}{\sigma_y^2}\, J_2(\boldsymbol{s}) - 1.\end{aligned} \tag{10.53}$$

The corresponding yield surface is that of the von Mises model with uniaxial yield stress σ_y:

$$\sqrt{3\, J_2(\boldsymbol{s})} = \sigma_y. \tag{10.54}$$

Geometric representation

Unlike isotropic models, whose yield functions can always be expressed in terms of principal stresses and the corresponding yield surfaces can be visualised in the three-dimensional principal stress space, yield surfaces for anisotropic models cannot be easily represented graphically. Anisotropic yield surfaces are truly six-dimensional hypersurfaces in the space of stress components. Nevertheless, visualisation of *projections* of such hypersurfaces on two- or three-dimensional subsets of the six-dimensional stress space is possible and can provide a very good insight into the properties of the anisotropic model. Two- and three-dimensional projections are obtained by fixing, respectively, four and three stress components and then plotting the corresponding yield locus on the subset of the two or three free stress components. In general, the two- or three-dimensional yield locus will change if the fixed stress components are changed. Thus, an appropriate visual study of anisotropic yield criteria requires plotting such projections with different combinations of fixed stress values.

In order to give the reader some visual insight into properties of the Hill criterion, we will plot here the corresponding yield surfaces under states of plane stress. Before proceeding to the graphical representation, it is worth remarking that at any given state of shear stress (defined by the components σ_{12}, σ_{23} and σ_{13} relative to the axes of material orthotropy), the yield surface defined by the Hill criterion (with material constants within the 'usable' range of the Hill model) in the three-dimensional σ_{11}-σ_{22}-σ_{33} space is a (generally elliptic) cylinder whose axis is the hydrostatic line ($\sigma_{11} = \sigma_{22} = \sigma_{33}$). The size of the cylinder cross-section (and its intersection with the plane stress space) depends upon the state of shear stress. For plane stress states (on plane $\{\boldsymbol{e}_1, \boldsymbol{e}_2\}$), the Hill yield surface is defined by

$$(F_1 + F_3)\,\sigma_{11}^2 + (F_1 + F_2)\,\sigma_{22}^2 - 2F_1\,\sigma_{11}\sigma_{22} + F_4\,\sigma_{12}^2 - \bar{\sigma}^2 = 0. \tag{10.55}$$

In order to study the effect of the material constants (the yield stresses) on the yield surface, we conveniently assume the following relations:

$$\sigma_{22}^0 = a_{22}\,\sigma_{11}^0; \quad \sigma_{33}^0 = a_{33}\,\sigma_{11}^0;$$
$$\sigma_{12}^0 = \frac{a_{12}}{\sqrt{3}}\,\sigma_{11}^0; \quad \sigma_{23}^0 = \frac{a_{23}}{\sqrt{3}}\,\sigma_{11}^0; \quad \sigma_{13}^0 = \frac{a_{13}}{\sqrt{3}}\,\sigma_{11}^0, \tag{10.56}$$

where a_{ij} are parameters defining all initial yield stresses of the model as a function of σ_{11}^0. Note that the von Mises surface, with uniaxial yield stress σ_{11}^0 is recovered if we set

$$a_{22} = a_{33} = a_{12} = a_{23} = a_{13} = 1. \tag{10.57}$$

Firstly, let us focus on the effect of the variation of direct yield stresses on the Hill yield surface. This effect is illustrated in Figures 10.5 and 10.6. In Figure 10.5, the Hill yield surface on the σ_{11}-σ_{22} space is plotted for different values of direct yield stress σ_{22}^0 (i.e. different values of a_{22}), assuming no shear stresses and

$$a_{33} = 1. \tag{10.58}$$

In this case (absence of shear stresses), the parameters a_{12}, a_{23} and a_{13} have no effect on the Hill yield function. For $a_{22} > 0.5$, the Hill surface is an ellipse intersecting the horizontal axis at ± 1 and the vertical axis at $\pm a_{22}$. The surface with $a_{22} = 1$ corresponds to that of the von Mises model. If a_{22} increases (see surface plotted for $a_{22} = 1.5$), the von Mises ellipse is stretched in the σ_{22} direction. If a_{22} decreases (refer to the surface with $a_{22} = 0.7$), the ellipse is compressed in the vertical direction but substantially stretched along its longer radius. In the limit, when $a_{22} = 0.5$ (one direct yield stress is half of the other two), the original ellipse degenerates into two parallel straight lines (two hyperplanes in the six-dimensional stress space). For $a_{22} < 0.5$ (see surface with $a_{22} = 0.3$), the yield locus produced by Hill's function is a set of two hyperbolic (non-convex) surfaces in stress space. Clearly, in such cases, the elastic domain becomes unbounded in some directions and does not correspond to physical behaviour. Thus, the Hill criterion is to be used only within certain limits of yield strength variation among the orthotropy directions. At this point, it is important to emphasise that the Hill criterion was originally proposed to model anisotropy of *formed steel* components. For such materials, the maximum variation of yield strength between the different orthotropy directions is typically less than about 5 to 10%. Under such conditions, the Hill criterion can provide reasonable approximations to the actual yield surfaces. In the next representation of the Hill surface shown in Figure 10.6, we illustrate the effect of the variation of the direct yield stress σ_{33}^0 (variation of a_{33}) in the absence of shear stresses and with $\sigma_{22}^0 = \sigma_{11}^0$ ($a_{22} = 1$). For $a_{33} > 0.5$, the Hill surface is always an ellipse intersecting the horizontal and vertical axis at ± 1. As σ_{33}^0 increases (see surface with $a_{33} = 1.5$), the ellipse stretches in the biaxial state direction. When σ_{33}^0 decreases (see surfaces with $a_{33} = 0.7$ and 0.6) the ellipse is compressed in the biaxial state direction and stretched in a pure shear ($\sigma_{11} = -\sigma_{22}$) direction. When $a_{33} = 0.5$ (one direct yield stress is half of the other two), the ellipse degenerates into two straight lines and becomes a hyperbola for $a_{33} < 0.5$. Finally, in Figure 10.7 we illustrate the effect of shear stresses on the Hill yield surface. Essentially, any increase in shear stress will shrink the yield surface isotropically (this effect is also present in the von Mises criterion and can only be seen if, as opposed to the usual representation in principal stress space, the surface is represented in the space of direct stresses along *fixed* axes). Obviously, if $\sigma_{12} = \bar{\sigma}\sigma_{12}^0$ (the shear stress has reached its yield limit) the σ_{11}-σ_{22} space surface degenerates to a point at $(0, 0)$.

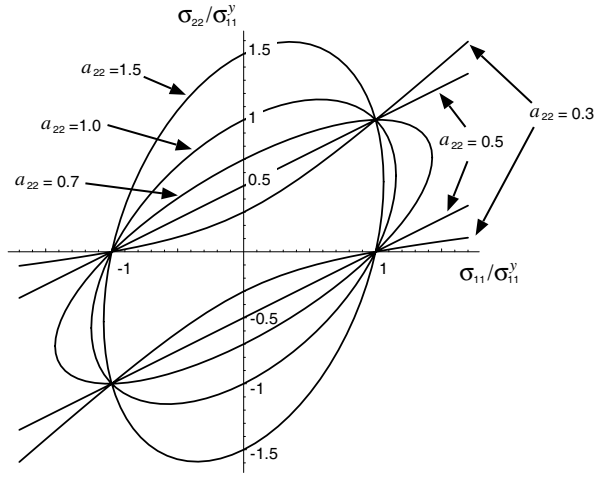

Figure 10.5. The Hill orthotropic criterion. Effect of variation of direct yield stress σ_{22}^0 on the yield surface. Surface plot for various values of a_{22} with no shear stresses and $a_{33} = 1$ ($\sigma_{33}^0 = \sigma_{11}^0$).

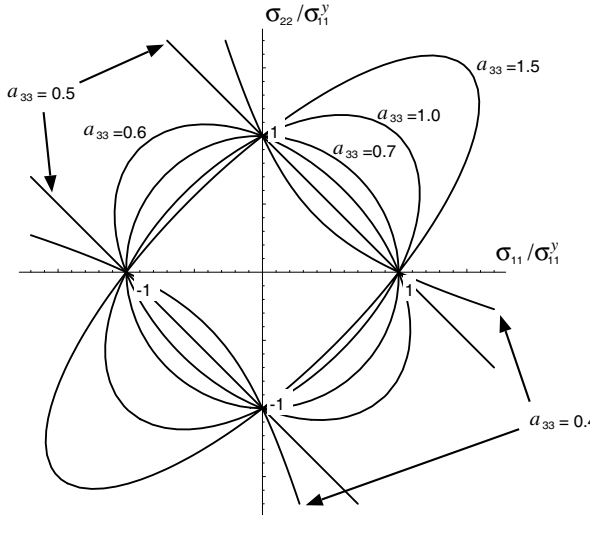

Figure 10.6. The Hill orthotropic criterion. Effect of variation of direct yield stress σ_{33}^0 (the transversal yield stress) on the yield surface. Surface plot for various values of a_{33} with no shear stresses and $a_{22} = 1$ ($\sigma_{22}^0 = \sigma_{11}^0$).

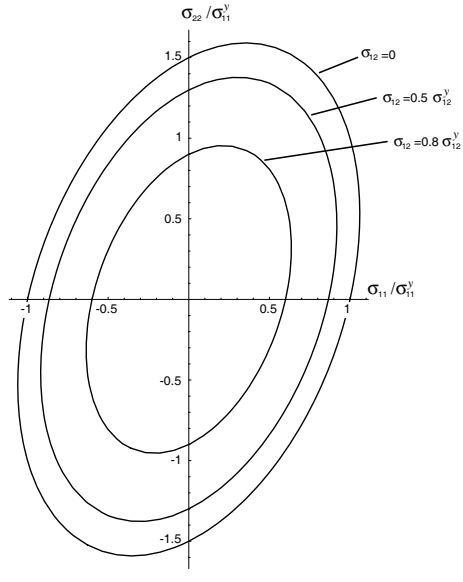

Figure 10.7. The Hill orthotropic criterion. Effect of shear stress on the yield surface. Surface plot for various values of σ_{12} with $\sigma_{23} = \sigma_{13} = 0$, $a_{22} = 1.5$ and $a_{12} = a_{33} = 1$.

Hardening law

Analogously to the standard strain-hardening von Mises model thoroughly discussed in Chapters 6, 7 and 9, *isotropic* strain hardening can be easily incorporated into the Hill model by assuming the relative yield stress $\bar{\sigma}$ in (10.43) to be a given function of the von Mises accumulated plastic strain, $\bar{\varepsilon}^p$; that is, we postulate

$$\bar{\sigma} = \bar{\sigma}(\bar{\varepsilon}^p). \tag{10.59}$$

The material in this case is assumed to remain orthotropic with constant axes of orthotropy. In addition, in view of (10.46), all six yield stresses of the Hill criterion will change in strict proportion (isotropically) as the accumulated plastic strain increases.

Remark 10.2. Since general straining of an initially orthotropic material is usually expected to change the yield stresses in different directions by different amounts, or even lead to loss of orthotropy, the model resulting from the above assumptions provides only a first approximation to the phenomenon of hardening. We remark, however, that the phenomenological modelling of hardening in plastically anisotropic materials is a complex issue which remains open at present. The approximation provided by simple laws of the above type can be very useful in the finite element analysis of plastically orthotropic materials and, undoubtedly, represents a substantial gain in predictive capability (as compared to the use of isotropic plasticity models) in situations where plastic anisotropy is an important feature of the material behaviour.

Hill's associative flow rule

The flow rule adopted by Hill (1950) in conjunction with the above orthotropic criterion is associative; that is, the plastic flow is given by the standard equation

$$\dot{\boldsymbol{\varepsilon}}^p = \dot{\gamma}\,\frac{\partial \Phi}{\partial \boldsymbol{\sigma}}. \tag{10.60}$$

Here, compact tensorial representation is not particularly convenient and the plastic flow rule is best presented in its equivalent component-wise format

$$\dot{\varepsilon}^p_{ij} = \dot{\gamma}\,\frac{\partial \Phi}{\partial \sigma_{ij}}. \tag{10.61}$$

Before presenting the final expressions, it is important to note that the shear stress contributions to (10.43) take into account the trivial identity

$$\sigma_{ij} = \sigma_{ji}, \quad i \neq j. \tag{10.62}$$

The actual contributions to Φ from the independent shear components, σ_{ij} $(i \neq j)$, of the stress tensor read

$$\tfrac{1}{2}[F_4(\sigma_{12}^2 + \sigma_{21}^2) + F_5(\sigma_{23}^2 + \sigma_{32}^2) + F_6(\sigma_{13}^2 + \sigma_{31}^2)]. \tag{10.63}$$

With the above considerations, Hill's associative flow rule is found to be given by

$$\begin{aligned}
\dot{\varepsilon}^p_{11} &= \dot{\gamma}\,2[F_1(\sigma_{11} - \sigma_{22}) + F_3(\sigma_{11} - \sigma_{33})],\\
\dot{\varepsilon}^p_{22} &= \dot{\gamma}\,2[F_1(\sigma_{22} - \sigma_{11}) + F_2(\sigma_{22} - \sigma_{33})],\\
\dot{\varepsilon}^p_{33} &= \dot{\gamma}\,2[F_2(\sigma_{33} - \sigma_{22}) + F_3(\sigma_{33} - \sigma_{11})],\\
\dot{\varepsilon}^p_{12} = \dot{\gamma}\,F_4\,\sigma_{12}, &\quad \dot{\varepsilon}^p_{23} = \dot{\gamma}\,F_5\,\sigma_{23}, \quad \dot{\varepsilon}^p_{13} = \dot{\gamma}\,F_6\,\sigma_{13}.
\end{aligned} \tag{10.64}$$

As expected, owing to the pressure-insensitivity of the Hill criterion, the above associative law is volume-preserving. Indeed, (10.64) implies

$$\operatorname{tr} \dot{\boldsymbol{\varepsilon}}^p \equiv \dot{\varepsilon}^p_{11} + \dot{\varepsilon}^p_{22} + \dot{\varepsilon}^p_{33} = 0. \tag{10.65}$$

10.3.2. TENSION–COMPRESSION DISTINCTION: THE HOFFMAN MODEL

For many materials, a marked difference is observed between yield stress levels in tension and compression (the Bauschinger effect). This phenomenon is particularly noticeable in some composite materials and is also commonly observed in worked metals. In order to model such effects in orthotropic materials, Hoffman (1967) proposed an extension to the Hill criterion described by the following yield function:[§]

$$\begin{aligned}
\Phi(\boldsymbol{\sigma}, \bar{\sigma}) = {} & C_1\,(\sigma_{11} - \sigma_{22})^2 + C_2\,(\sigma_{22} - \sigma_{33})^2 + C_3\,(\sigma_{33} - \sigma_{11})^2\\
& + C_4\,\sigma_{12}^2 + C_5\,\sigma_{23}^2 + C_6\,\sigma_{13}^2 + C_7\,\sigma_{11} + C_8\,\sigma_{22} + C_9\,\sigma_{33} - \bar{\sigma}^2,
\end{aligned} \tag{10.66}$$

[§]This function was in fact proposed by Hoffman (1967) originally to define a *fracture* criterion for brittle materials, with no reference to plastic flow modelling. What we refer to as the Hoffman model here, is an extension of the Hill elastoplastic model with yield criterion and plastic flow rule based on Hoffman's function (10.66).

where $\bar{\sigma}$ is the non-dimensional relative yield stress (analogous to that of the Hill criterion) and $C_1, C_2, \ldots, C_9$ are material constants defined as

$$\begin{aligned} C_1 &= \frac{1}{2}\left(\frac{1}{\sigma_{11}^t\sigma_{11}^c} + \frac{1}{\sigma_{22}^t\sigma_{22}^c} - \frac{1}{\sigma_{33}^t\sigma_{33}^c}\right); \\ C_2 &= \frac{1}{2}\left(\frac{-1}{\sigma_{11}^t\sigma_{11}^c} + \frac{1}{\sigma_{22}^t\sigma_{22}^c} + \frac{1}{\sigma_{33}^t\sigma_{33}^c}\right); \\ C_3 &= \frac{1}{2}\left(\frac{1}{\sigma_{11}^t\sigma_{11}^c} - \frac{1}{\sigma_{22}^t\sigma_{22}^c} + \frac{1}{\sigma_{33}^t\sigma_{33}^c}\right), \end{aligned} \tag{10.67}$$

with σ_{ii}^t and σ_{ii}^c (no summation on repeated indices) denoting the initial (i.e. when $\bar{\sigma} = 1$) direct yield stresses along the orthotropy direction i, respectively in tension and compression, and

$$C_4 = \frac{1}{(\sigma_{12}^0)^2}; \quad C_5 = \frac{1}{(\sigma_{23}^0)^2}; \quad C_6 = \frac{1}{(\sigma_{13}^0)^2}, \tag{10.68}$$

and

$$C_7 = \frac{\sigma_{11}^c - \sigma_{11}^t}{\sigma_{11}^c\sigma_{11}^t}; \quad C_8 = \frac{\sigma_{22}^c - \sigma_{22}^t}{\sigma_{22}^c\sigma_{22}^t}; \quad C_9 = \frac{\sigma_{33}^c - \sigma_{33}^t}{\sigma_{33}^c\sigma_{33}^t}. \tag{10.69}$$

The constants σ_{12}^0, σ_{23}^0 and σ_{13}^0 have the same meaning as in the Hill criterion, i.e. they denote the initial yield stresses in states of pure shear on the planes of orthotropy.

Remark 10.3 (Hill criterion as a particular case). If for each principal direction of orthotropy the direct yield stress in tension coincides with the direct yield stress in compression, i.e. if we set

$$\sigma_{11}^c = \sigma_{11}^t = \sigma_{11}^0; \quad \sigma_{22}^c = \sigma_{22}^t = \sigma_{22}^0; \quad \sigma_{33}^c = \sigma_{33}^t = \sigma_{33}^0, \tag{10.70}$$

then $C_7 = C_8 = C_9 = 0$ and the constants $C_1, \ldots, C_6$ coincide with the constants $F_1, \ldots, F_6$ of (10.43). In this case, the Hill criterion is recovered. However, it should be noted that, in general, the Hoffman criterion is (unlike the Hill criterion) *pressure-sensitive*. Indeed, under a state of pure hydrostatic pressure ($\sigma_{11} = \sigma_{22} = \sigma_{33} = p$), the contribution of the linear terms on the direct stresses to Φ in (10.66) will be

$$(C_7 + C_8 + C_9)p. \tag{10.71}$$

This contribution – a linear function of the hydrostatic pressure – is identical to that of the Drucker–Prager criterion (refer to expression (6.121), page 167). The constraint

$$C_7 + C_8 + C_9 = 0 \tag{10.72}$$

is the necessary and sufficient condition for the Hoffman criterion to be pressure-insensitive.

In its general form (within the range of applicability of the criterion), the Hoffman yield surface is an elliptic cone in the σ_{11}-σ_{22}-σ_{33} space. The cone intersects the σ_{11}, σ_{22} and σ_{33} axes at the corresponding prescribed values of (tensile and compressive) direct yield stresses. A graphical representation of the Hoffman criterion is shown in Figure 10.8. Again, only the intersection of the yield surface with the σ_{11}-σ_{22} plane, in the absence of shear stresses, is

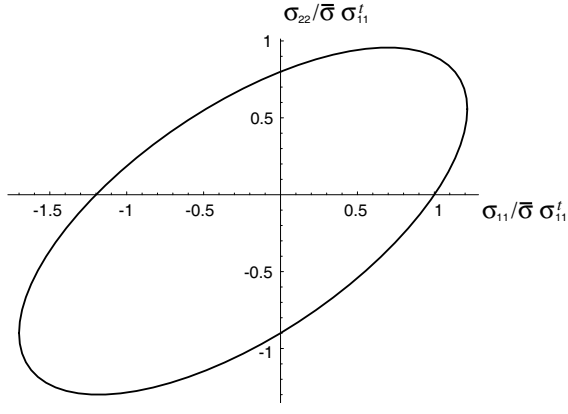

Figure 10.8. The Hoffman orthotropic criterion.

plotted. For illustration purposes only, the following relations have been chosen:

$$\sigma_{11}^c = 1.2\,\sigma_{11}^t; \quad \sigma_{22}^c = 0.9\,\sigma_{11}^t; \quad \sigma_{22}^t = 0.8\,\sigma_{11}^t; \\ \sigma_{33}^c = \sigma_{11}^c; \quad \sigma_{33}^t = \sigma_{11}^t. \tag{10.73}$$

As for the Hill criterion (refer to Figure 10.7), the Hoffman surface shrinks isotropically with an increase in shear stresses. The effect of (isotropic) hardening can also be incorporated into the Hoffman criterion by assuming $\bar{\sigma}$ to be a function of the accumulated plastic strain.

Again, it is important to observe that (as for the Hill criterion) the Hoffman model can only be used within certain limits of yield strength variation among the directions of orthotropy. Excessive variations of direct (tensile or compressive) yield stress can cause the originally elliptic surface to degenerate into a hyperbola that does not model the actual behaviour of solids.

Flow rule

Here, an associative flow rule is also postulated. Analogously to (10.64), the associative component-wise plastic flow equations for the Hoffman model are given by

$$\begin{aligned} \dot{\varepsilon}_{11}^p &= \dot{\gamma}\,[C_7 + 2C_1(\sigma_{11} - \sigma_{22}) + 2C_3(\sigma_{11} - \sigma_{33})], \\ \dot{\varepsilon}_{22}^p &= \dot{\gamma}\,[C_8 + 2C_1(\sigma_{22} - \sigma_{11}) + 2C_2(\sigma_{22} - \sigma_{33})], \\ \dot{\varepsilon}_{33}^p &= \dot{\gamma}\,[C_9 + 2C_2(\sigma_{33} - \sigma_{22}) + 2C_3(\sigma_{33} - \sigma_{11})], \\ \dot{\varepsilon}_{12}^p &= \dot{\gamma}\,C_4\,\sigma_{12}, \quad \dot{\varepsilon}_{23}^p = \dot{\gamma}\,C_5\,\sigma_{23}, \quad \dot{\varepsilon}_{13}^p = \dot{\gamma}\,C_6\,\sigma_{13}. \end{aligned} \tag{10.74}$$

Remark 10.4 (Non-isochoric plastic flow). As a result of the pressure-sensitivity of the Hoffman criterion, the above associative flow rule is *not volume-preserving* in general. The volumetric plastic strain rate for the present model is

$$\operatorname{tr} \dot{\boldsymbol{\varepsilon}}^p \equiv \dot{\varepsilon}_{11}^p + \dot{\varepsilon}_{22}^p + \dot{\varepsilon}_{33}^p = \dot{\gamma}\,(C_7 + C_8 + C_9), \tag{10.75}$$

and the plastic flow is isochoric if and only if constraint (10.72) holds.

10.3.3. IMPLEMENTATION OF THE HOFFMAN MODEL

The computational implementation of the Hoffman model is described in what follows. For simplicity, the discussion will be limited to the plane strain and axisymmetric cases. The extension to the full three-dimensional situation is trivial. Early implementations of the Hill and Hoffman anisotropic models are described, respectively, by de Borst and Feenstra (1990) and Schellekens and de Borst (1990). A plane stress implementation of the Hoffman model in the context of explicit dynamics finite element analysis is given by Koh *et al.* (1995).

The orthotropic elastic law

As plastically orthotropic composites usually also present a marked elastic orthotropy, we shall assume here an *orthotropic elasticity* law. Clearly, in this case it makes sense to consider an elastic law whose planes of symmetry coincide with the planes of symmetry of the Hoffman criterion. Using the finite element array notation, the stress–elastic strain relation then reads

$$\boldsymbol{\sigma} = \mathbf{D}\ \boldsymbol{\varepsilon}^e, \tag{10.76}$$

where

$$\boldsymbol{\sigma}^e = [\sigma_{11}\ \ \sigma_{22}\ \ \sigma_{12}\ \ \sigma_{33}]^T; \quad \boldsymbol{\varepsilon}^e = [\varepsilon^e_{11}\ \ \varepsilon^e_{22}\ \ 2\varepsilon^e_{12}\ \ \varepsilon^e_{33}]^T, \tag{10.77}$$

and $\mathbf{D}$ denotes the *orthotropic elasticity matrix* given by

$$\mathbf{D} = \begin{bmatrix} D_{11} & D_{12} & 0 & D_{13} \\ D_{12} & D_{22} & 0 & D_{23} \\ 0 & 0 & D_{44} & 0 \\ D_{13} & D_{23} & 0 & D_{33} \end{bmatrix}, \tag{10.78}$$

with

$$D_{ii} = \frac{E_i(1-\nu_{jk}\nu_{kj})}{(1-\nu_{ki}\nu_{ik})(1-\nu_{jk}\nu_{kj}) - (\nu_{ij}+\nu_{ik}\nu_{kj})(\nu_{ji}+\nu_{jk}\nu_{ki})} \tag{10.79}$$

for $i = 1, 2, 3$ (no summation on the repeated index) and (i, j, k) denoting cyclic permutations of $(1, 2, 3)$,

$$D_{ij} = \frac{\nu_{ji}+\nu_{jk}\nu_{ki}}{1-\nu_{jk}\nu_{kj}}\, D_{ii} \tag{10.80}$$

for $i \neq j$ and, again, no summation on the repeated index, and

$$D_{44} = G_{12}. \tag{10.81}$$

The total number of independent elastic constants is nine (in the full three-dimensional case). These are: the Young's moduli, E_1, E_2 and E_3, associated with directions 1, 2 and 3 of orthotropy respectively; the shear moduli, G_{12}, G_{23} and G_{31} associated, respectively, with planes 12, 23 and 31 and satisfying

$$G_{ij} = G_{ji}; \tag{10.82}$$

and three Poisson's ratios, ν_{12}, ν_{23} and ν_{31}, where ν_{ij} is defined as the ratio between the contraction in direction j and extension in direction i under a uniaxial stress state along i.

The following relation applies:

$$\nu_{ji} = \nu_{ij} \, \frac{E_j}{E_i}. \tag{10.83}$$

In the plane strain/axisymmetric case, with the elasticity operator represented in (10.78), the transverse shear moduli G_{23} and G_{31} are not required.

Elastic trial state

The computation of the elastic trial state proceeds as usual. That is, we compute

$$\boldsymbol{\sigma}^{\text{trial}} = \mathbf{D} \, \boldsymbol{\varepsilon}^{e \, \text{trial}}, \tag{10.84}$$

where, clearly, the $\mathbf{D}$ matrix here is the orthotropic operator (10.78). The trial accumulated plastic strain (isotropic hardening state variable) is

$$\bar{\varepsilon}^{p \, \text{trial}} = \bar{\varepsilon}^{p}_{n}. \tag{10.85}$$

If the trial state is outside the elastic domain defined by the yield function (10.66), the return mapping described below is applied.

Return-mapping algorithm

For computer implementation purposes, it is convenient to write the Hoffman yield function (10.66) in the following equivalent form in terms of the array of stress components:

$$\Phi(\boldsymbol{\sigma}, \bar{\sigma}) = \tfrac{1}{2} \, \boldsymbol{\sigma}^T \mathbf{P} \boldsymbol{\sigma} + \mathbf{q}^T \boldsymbol{\sigma} - \bar{\sigma}^2, \tag{10.86}$$

where

$$\mathbf{P} = 2 \begin{bmatrix} C_1 + C_3 & -C_1 & 0 & -C_3 \\ -C_1 & C_2 + C_1 & 0 & -C_2 \\ 0 & 0 & C_4 & 0 \\ -C_3 & -C_2 & 0 & C_3 + C_2 \end{bmatrix} \tag{10.87}$$

and

$$\mathbf{q} = [\, C_7 \quad C_8 \quad 0 \quad C_9 \,]^T. \tag{10.88}$$

With the above notation, the flow rule (10.74) can be equivalently expressed in terms of the engineering plastic strain rate array as

$$\dot{\boldsymbol{\varepsilon}}^p = \dot{\gamma} \, (\mathbf{P} \boldsymbol{\sigma} + \mathbf{q}). \tag{10.89}$$

The rate of accumulated plastic strain, in turn, can be represented as

$$\begin{aligned} \dot{\bar{\varepsilon}}^p &\equiv \sqrt{\tfrac{2}{3} \, \dot{\boldsymbol{\varepsilon}}^p : \dot{\boldsymbol{\varepsilon}}^p} = \dot{\gamma} \, \sqrt{\tfrac{2}{3} \, (\dot{\boldsymbol{\varepsilon}}^p)^T \, \mathbf{Z} \, \dot{\boldsymbol{\varepsilon}}^p} \\ &= \dot{\gamma} \, \sqrt{\tfrac{2}{3} \, (\mathbf{P} \boldsymbol{\sigma} + \mathbf{q})^T \, \mathbf{Z} \, (\mathbf{P} \boldsymbol{\sigma} + \mathbf{q})}, \end{aligned} \tag{10.90}$$

where we have used the definition

$$\mathbf{Z} = \begin{bmatrix} 1 & 0 & 0 & 0 \\ 0 & 1 & 0 & 0 \\ 0 & 0 & \frac{1}{2} & 0 \\ 0 & 0 & 0 & 1 \end{bmatrix}. \tag{10.91}$$

With the above relations at hand, a direct particularisation of the general return-mapping equations (7.25) (page 196) is obtained as

$$\left\{ \begin{array}{c} \boldsymbol{\varepsilon}^e_{n+1} - \boldsymbol{\varepsilon}^{e\,\mathrm{trial}} + \Delta\gamma\,(\mathbf{P}\boldsymbol{\sigma}_{n+1} + \mathbf{q}) \\ \bar{\varepsilon}^p_{n+1} - \bar{\varepsilon}^p_n - \Delta\gamma[\frac{2}{3}\,(\mathbf{P}\boldsymbol{\sigma}_{n+1} + \mathbf{q})^T\,\mathbf{Z}\,(\mathbf{P}\boldsymbol{\sigma}_{n+1} + \mathbf{q})]^{\frac{1}{2}} \\ \frac{1}{2}\,\boldsymbol{\sigma}^T_{n+1}\mathbf{P}\boldsymbol{\sigma}_{n+1} + \mathbf{q}^T\boldsymbol{\sigma}_{n+1} - [\bar{\sigma}(\bar{\varepsilon}^p_{n+1})]^2 \end{array} \right\} = \left\{ \begin{array}{c} \mathbf{0} \\ 0 \\ 0 \end{array} \right\}. \tag{10.92}$$

Single-equation return mapping

Analogously to the implementation of the von Mises model, the return mapping here can also be reduced to the solution of a single equation for the plastic multiplier, $\Delta\gamma$. To obtain the reduced equation, we start by noting that, by using the linear elastic law, the first equation of system (10.92) can be expressed, after a straightforward manipulation, as

$$\boldsymbol{\sigma}_{n+1} = \boldsymbol{\sigma}(\Delta\gamma) \equiv (\mathbf{I} + \Delta\gamma\,\mathbf{D}\mathbf{P})^{-1}(\boldsymbol{\sigma}^{\mathrm{trial}} - \Delta\gamma\,\mathbf{D}\mathbf{q}); \tag{10.93}$$

that is, the updated stress, $\boldsymbol{\sigma}_{n+1}$ is a function of $\Delta\gamma$, exclusively. Further, introduction of the above function in the second equation of (10.92) gives

$$\bar{\varepsilon}^p_{n+1} = \bar{\varepsilon}^p(\Delta\gamma) \equiv \bar{\varepsilon}^p_n + \Delta\gamma\{\tfrac{2}{3}\,[\mathbf{P}\boldsymbol{\sigma}(\Delta\gamma) + \mathbf{q}]^T\,\mathbf{Z}\,[\mathbf{P}\boldsymbol{\sigma}(\Delta\gamma) + \mathbf{q}]\}^{\frac{1}{2}}. \tag{10.94}$$

Finally, with the substitution of the last two expressions in the third equation of (10.92) – the discretised plastic consistency – the original return-mapping system is reduced to the following nonlinear scalar equation for $\Delta\gamma$:

$$\tilde{\Phi}(\Delta\gamma) \equiv \tfrac{1}{2}\,[\boldsymbol{\sigma}(\Delta\gamma)]^T\mathbf{P}\boldsymbol{\sigma}(\Delta\gamma) + \mathbf{q}^T\boldsymbol{\sigma}(\Delta\gamma) - [\bar{\sigma}(\bar{\varepsilon}^p(\Delta\gamma))]^2 = 0. \tag{10.95}$$

In summary, the stress-updating procedure for the Hoffman model comprises the solution of (10.95), followed by the update of stress and accumulated plastic strain according to (10.93) and (10.94), respectively.

Newton–Raphson solution

In the Newton–Raphson iterative scheme to solve (10.95), the k^{th} guess for the solution $\Delta\gamma$ is obtained as

$$\Delta\gamma^{(k)} = \Delta\gamma^{(k-1)} + \delta\Delta\gamma^{(k)}, \tag{10.96}$$

where

$$\delta\Delta\gamma^{(k)} = -\left.\frac{\tilde{\Phi}(\Delta\gamma)}{\mathrm{d}\tilde{\Phi}/\mathrm{d}\Delta\gamma}\right|^{(k-1)}. \tag{10.97}$$

The derivative of $\tilde{\Phi}$ is given by

$$\frac{\mathrm{d}\tilde{\Phi}}{\mathrm{d}\Delta\gamma} = [\mathbf{P}\boldsymbol{\sigma}(\Delta\gamma) + \mathbf{q}]^T \frac{\mathrm{d}\boldsymbol{\sigma}}{\mathrm{d}\Delta\gamma} - 2\,\bar{\sigma}(\Delta\gamma)\,\bar{H}\,\frac{\mathrm{d}\bar{\varepsilon}^p}{\mathrm{d}\Delta\gamma}, \tag{10.98}$$

where $\bar{H} \equiv \mathrm{d}\bar{\sigma}/\mathrm{d}\bar{\varepsilon}^p$ is the slope of the (non-dimensional) hardening curve. To obtain an explicit expression for the derivative of function $\boldsymbol{\sigma}$ defined by (10.93), we need to use formula (vii) of page 36. A straightforward manipulation then gives

$$\frac{\mathrm{d}\boldsymbol{\sigma}}{\mathrm{d}\Delta\gamma} = -(\mathbf{I} + \Delta\gamma\,\mathbf{DP})^{-1}\mathbf{D}\,[\mathbf{P}\,\boldsymbol{\sigma}(\Delta\gamma) + \mathbf{q}]. \tag{10.99}$$

With the above expressions at hand, the derivation of a complete explicit formula for the derivative of $\tilde{\Phi}$ is a rather simple exercise which we shall leave for the interested reader.

The elastoplastic consistent tangent

As in the modified Cam-Clay implementation presented earlier in this chapter (refer to the text preceding equation (10.23), page 408), to derive the elastoplastic consistent tangent operator for the above implementation of the Hoffman model, we shall follow the general procedure of Section 7.4.4 (from page 238). Here, we start by differentiating the system (10.92), which together with the elastic law, gives the following linearised system in finite element array notation:

$$\begin{bmatrix} \mathbf{D}^{-1} + \Delta\gamma\mathbf{P} & 0 & \mathbf{N} \\ -\dfrac{2\Delta\gamma}{3\eta}\mathbf{N}^T\mathbf{ZP} & 1 & -\eta \\ \mathbf{N}^T & -2\,\bar{\sigma}\bar{H} & 0 \end{bmatrix} \begin{Bmatrix} \mathrm{d}\boldsymbol{\sigma}_{n+1} \\ \mathrm{d}\bar{\varepsilon}^p_{n+1} \\ \mathrm{d}\Delta\gamma \end{Bmatrix} = \begin{Bmatrix} \mathrm{d}\boldsymbol{\varepsilon}^{e\,\mathrm{trial}} \\ 0 \\ 0 \end{Bmatrix}, \tag{10.100}$$

where $\bar{\sigma} = \bar{\sigma}(\bar{\varepsilon}^p_{n+1})$ and $\bar{H}$ is the non-dimensional hardening modulus

$$\bar{H} = \frac{\mathrm{d}\bar{\sigma}}{\mathrm{d}\bar{\varepsilon}^p}, \tag{10.101}$$

also evaluated at $\bar{\varepsilon}^p_{n+1}$. The flow vector $\mathbf{N}$ is given by

$$\mathbf{N} = \mathbf{P}\boldsymbol{\sigma}_{n+1} + \mathbf{q}, \tag{10.102}$$

and the scalar η is defined as

$$\eta = \sqrt{\tfrac{2}{3}\mathbf{N}^T\mathbf{Z}\,\mathbf{N}}. \tag{10.103}$$

Finally, with the inversion of (10.100) we obtain

$$\mathbf{D}^{ep} \equiv \frac{\mathrm{d}\boldsymbol{\sigma}_{n+1}}{\mathrm{d}\boldsymbol{\varepsilon}^{e\,\mathrm{trial}}} = \left[\mathbf{D}^{-1} + \Delta\gamma\,\mathbf{P} + \frac{1}{2\bar{\sigma}\bar{H}\eta}\,\mathbf{N}\mathbf{N}^T - \frac{2\Delta\gamma}{3\eta^2}\,\mathbf{N}^T\mathbf{N}\mathbf{Z}\mathbf{P}\right]^{-1}. \tag{10.104}$$

The above operator is clearly unsymmetric. Its non-symmetry is a consequence of the fact that the adopted hardening rule is non-associative (despite the associativity of the plastic

flow rule). Refer to the comments made in Section 7.4.6, page 243. Note that the above formula is analogous to that given by (7.149) for the von Mises isotropically hardening model. Its use, in this format, is restricted strictly to hardening models ($\bar{H} \neq 0$) owing to the presence of the hardening modulus in the denominator of the third summand of the term within square brackets. For use under the assumption of perfect plasticity ($H = 0$), an alternative representation can be obtained following completely analogous steps to those leading to expression (7.148). This will be left as an exercise for the interested reader.

10.3.4. THE BARLAT–LIAN MODEL FOR SHEET METALS

The Barlat–Lian criterion (Barlat and Lian, 1989) has been proposed to model the behaviour of orthotropic metallic sheets (typically rolled materials) under plane stress. Unlike the other plasticity models discussed in this book, whose equations are firstly formulated in the six-dimensional stress space and corresponding plane stress versions are subsequently addressed within the framework of Chapter 9, the Barlat–Lian criterion was originally defined in plane stress format. The corresponding yield function, written at the outset exclusively in terms of in-plane components of the stress tensor, reads

$$\Phi(\boldsymbol{\sigma}, \sigma_{11}^y) = f(\boldsymbol{\sigma}) - 2\,(\sigma_{11}^y)^M, \tag{10.105}$$

where

$$f(\boldsymbol{\sigma}) \equiv a|K_1 + K_2|^M + a|K_1 - K_2|^M + (2-a)|2\,K_2|^M, \tag{10.106}$$

with

$$K_1 = \frac{\sigma_{11} + h\,\sigma_{22}}{2}; \quad K_2 = \sqrt{\left(\frac{\sigma_{11} - h\,\sigma_{22}}{2}\right)^2 + b^2\,\sigma_{12}^2}, \tag{10.107}$$

where M, a, b and h are material constants and σ_{11}^y is the uniaxial yield stress in the principal orthotropy direction 1. The yield function (10.105) is convex (Barlat and Lian, 1989) if

$$M > 1, \quad a, b, h > 0, \quad a < 2. \tag{10.108}$$

To give the reader an idea of realistic values for these constants, the following have been determined by Lege *et al.* (1989) for an aluminium alloy:

$$M = 8, \quad a = 1.24, \quad b = 1.02, \quad h = 1.15. \tag{10.109}$$

The constant M defines the curvature of the yield surface. This can be seen in Figure 10.9 where the projection of the Barlat–Lian yield surface on the σ_{11}-σ_{22} plane is shown (in the absence of shear stresses) for different values of M and $a = h = 1$ (note that the value of b is immaterial in the absence of shear). We remark that the criterion becomes isotropic when $a = b = h = 1$. Under such a condition, the standard von Mises locus is recovered when $M = 2$ and the Tresca yield locus is recovered for $M = 1$ and $M \to \infty$. The parameter h relates the uniaxial yield strength, σ_{22}^y, in the principal orthotropy direction 2 with that of direction 1; that is,

$$\sigma_{22}^y = \frac{\sigma_{11}^y}{h}. \tag{10.110}$$

The effect of the choice of h on the Barlat–Lian yield surface is illustrated in Figure 10.10(a). The effect of constant a is shown in Figure 10.10(b). Similarly to the previously discussed

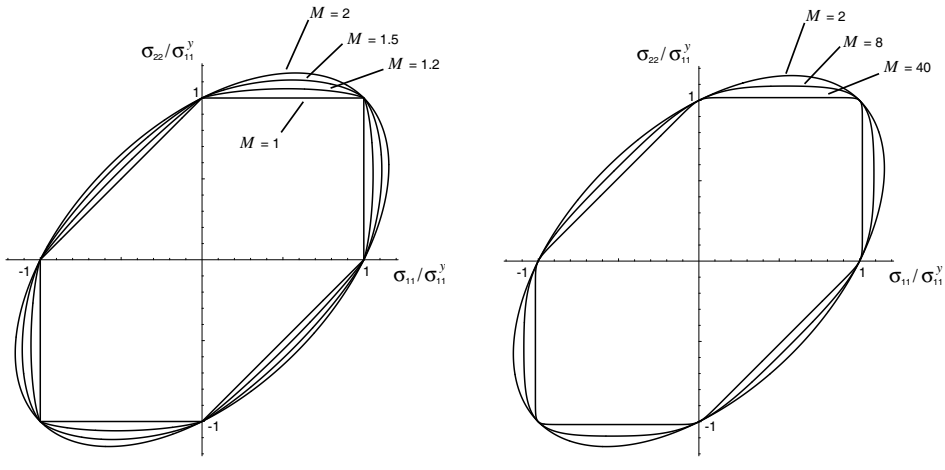

Figure 10.9. The Barlat–Lian criterion. Yield surfaces on σ_{11}-σ_{22} plane (in the absence of shear stress) for various values of M with $a = h = 1$.

Hill and Hoffman criteria, the presence of shear stresses will shrink the Barlat–Lian yield surface. This effect is illustrated in Figure 10.11, where we plot yield surfaces obtained with $M = 8$, $a = b = 1$ and $h = 2/3$ at different levels of shear stress. We remark that (not shown in Figure 10.11) an increase (decrease) in constant b will increase (decrease) the rate at which the surface shrinks with increasing shear stress.

For the purposes of computational implementation of the model, it turns out to be more convenient to describe the yield criterion for the Barlat–Lian model equivalently in terms of the following alternative definition of the yield function:

$$\Phi(\boldsymbol{\sigma}, \sigma_{11}^y) = g(\boldsymbol{\sigma}) - \sigma_{11}^y, \tag{10.111}$$

where

$$g(\boldsymbol{\sigma}) \equiv [\tfrac{1}{2} f(\boldsymbol{\sigma})]^{1/M}. \tag{10.112}$$

Note that the yield function now has dimension of stress. In the original definition (10.105), the yield function has dimension of stress to the power M, which may produce computationally intractable numbers for large values of material constant M.

Hardening law

Analogously to the Hill and Hoffman criteria, isotropic hardening can be incorporated into the present model by letting σ_{11}^y be a prescribed function of a scalar strain-like hardening internal variable, α:

$$\sigma_{11}^y = \sigma_{11}^y(\alpha). \tag{10.113}$$

Here we take the yield function (10.111) as the plastic potential and assume the evolution of the isotropic hardening variable to be governed by the standard relation

$$\dot{\alpha} = -\dot{\gamma} \frac{\partial \Phi}{\partial \sigma_{11}^y} = \dot{\gamma}. \tag{10.114}$$

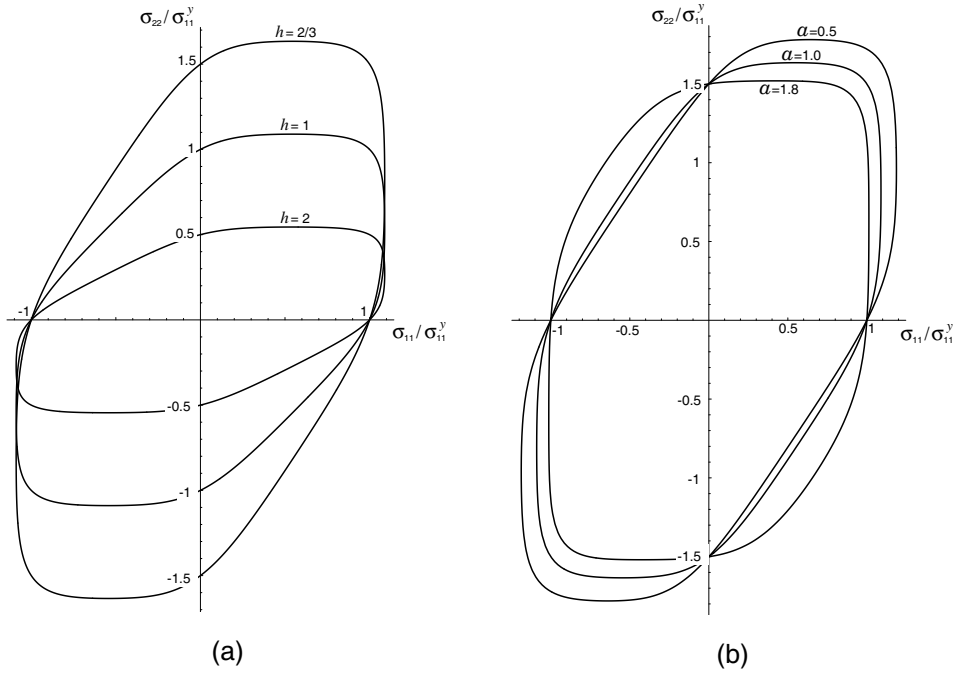

Figure 10.10. The Barlat–Lian criterion. Yield surfaces in the absence of shear for $M = 8$: (a) effect of parameter h with $a = 1$; (b) effect of parameter a with $h = 2/3$.

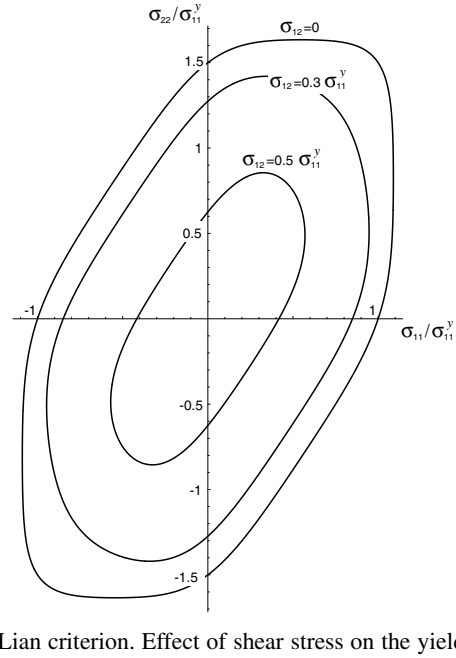

Figure 10.11. The Barlat–Lian criterion. Effect of shear stress on the yield surface for $M = 8$, $a = 1$, $h = 2/3$ and $b = 1$.

Flow rule

The Barlat–Lian yield function (10.111) is represented analogously to the plane stress-projected von Mises yield function given in (9.41)$_3$, page 372. The *in-plane* associative plastic strain rate is given simply by

$$\dot{\boldsymbol{\varepsilon}}^p = \dot{\gamma}\, \boldsymbol{N}, \tag{10.115}$$

where

$$\boldsymbol{N} \equiv \frac{\partial \Phi}{\partial \boldsymbol{\sigma}} = \frac{\partial g}{\partial \boldsymbol{\sigma}} = \frac{1}{2M}\left(\frac{f}{2}\right)^{(1-M)/M} \frac{\partial f}{\partial \boldsymbol{\sigma}}. \tag{10.116}$$

Equivalently, in component form, we have

$$\dot{\varepsilon}^p_{\alpha\beta} = \dot{\gamma}\, \frac{1}{2M}\left(\frac{f}{2}\right)^{(1-M)/M} \frac{\partial f}{\partial \sigma_{\alpha\beta}}, \quad \alpha, \beta = 1, 2. \tag{10.117}$$

The corresponding explicit formulae for the derivatives of f are

$$\begin{aligned}\frac{\partial f}{\partial \sigma_{11}} = \frac{M}{2}\Bigg\{ & a(K_1 - K_2)\,|K_1 - K_2|^{M-2}\left(1 - \frac{\sigma_{11} - h\sigma_{22}}{2K_2}\right) \\ & + a(K_1 + K_2)\,|K_1 + K_2|^{M-2}\left(1 - \frac{\sigma_{11} - h\sigma_{22}}{2K_2}\right) \\ & + 2^M(2-a)K_2^{M-1}\,\frac{\sigma_{11} - h\sigma_{22}}{2K_2}\Bigg\},\end{aligned} \tag{10.118}$$

$$\begin{aligned}\frac{\partial f}{\partial \sigma_{22}} = \frac{Mh}{2}\Bigg\{ & a(K_1 - K_2)\,|K_1 + K_2|^{M-2}\left(1 - \frac{\sigma_{11} - h\sigma_{22}}{2K_2}\right) \\ & + a(K_1 + K_2)\,|K_1 - K_2|^{M-2}\left(1 - \frac{\sigma_{11} - h\sigma_{22}}{2K_2}\right) \\ & - 2^M(2-a)K_2^{M-1}\,\frac{\sigma_{11} - h\sigma_{22}}{2K_2}\Bigg\},\end{aligned} \tag{10.119}$$

$$\begin{aligned}\frac{\partial f}{\partial \sigma_{12}} = \frac{Mb^2\sigma_{12}}{2K_2}\{ & a(K_1 + K_2)\,|K_1 + K_2|^{M-2} \\ & - a(K_1 - K_2)\,|K_1 - K_2|^{M-2} + 2(2-a)(2K_2)^{M-1}\}.\end{aligned} \tag{10.120}$$

Note that, in deriving (10.120), we have taken into account the tensorial nature of the shear stress contribution in (10.105) (refer to the comments surrounding expression (10.63)). The thickness plastic strain rate is obtained by imposing plastic incompressibility and the transversal plastic shear strain rates are assumed to vanish. Thus, the complete set of plastic flow equations comprises (10.117)–(10.120) together with the out-of plane rates

$$\dot{\varepsilon}^p_{33} = -\dot{\varepsilon}^p_{11} - \dot{\varepsilon}^p_{22}, \quad \dot{\varepsilon}^p_{13} = \dot{\varepsilon}^p_{23} = 0. \tag{10.121}$$

Finally, to complete the definition of the model, we assume the material to be elastically isotropic. Then, following the procedure applied to the plane stress-projected von Mises model, all out-of-plane strain components can be recovered *a posteriori* as functions of the in-plane elastic and plastic strains according to relations (9.37)–(9.40) (refer to page 371).

10.3.5. IMPLEMENTATION OF THE BARLAT–LIAN MODEL

The implicit elastic predictor/plastic corrector computational implementation of the (isotropically strain hardening) Barlat–Lian model, including the corresponding consistent tangent operator, was originally proposed by Dutko *et al.* (1993). The implementation is a particular case of the general methodology adopted throughout this book but, as we shall see, requires the inclusion of an extra procedure – a *line-search* algorithm – to expand the radius of convergence of the Newton–Raphson scheme used to solve the return mapping equations (refer to Remark 7.3, page 199, for a discussion on the possible need for strategies of this nature). The corresponding algorithm and associated consistent tangent operator are described in the following.

The return-mapping equations

The elastic predictor stage of the algorithm in the present case is clearly identical to that of the plane stress-projected von Mises model as described in Subsection 9.4.2 (refer to Box 9.4, page 377) and, therefore, requires no further consideration.

The return mapping is a specialisation of (7.25) (page 196), requiring the solution of the algebraic system of equations

$$\left\{ \begin{array}{c} \boldsymbol{\varepsilon}^e_{n+1} - \boldsymbol{\varepsilon}^{e\,\mathrm{trial}} + \Delta\gamma\, \boldsymbol{N}_{n+1} \\ \alpha_{n+1} - \alpha_n - \Delta\gamma \\ \Phi(\boldsymbol{\sigma}(\varepsilon^e_{n+1}), \kappa(\alpha_{n+1})) \end{array} \right\} = \left\{ \begin{array}{c} \mathbf{0} \\ 0 \\ 0 \end{array} \right\} \tag{10.122}$$

for the unknowns $\boldsymbol{\varepsilon}^e_{n+1}$, α_{n+1} and $\Delta\gamma$, where $\boldsymbol{N}_{n+1}$ is the flow vector (10.116) evaluated at the updated state. We remark that only the *in-plane* components of the elastic strain take part in the above equation. For convenience in the description of the return-mapping algorithm we have adopted, here and in what follows, the notation

$$\kappa \equiv \sigma^y_{11}. \tag{10.123}$$

In the derivation of the return mapping presented below, we shall assume linear hardening, i.e.

$$\kappa = \kappa_0 + H\ \alpha, \tag{10.124}$$

where H is the hardening modulus. Then, in the discrete setting, the evolution of κ reads

$$\kappa_{n+1} = \kappa_n + H\ \Delta\gamma. \tag{10.125}$$

With this relation and taking into account the linear elasticity law, the return-mapping equation set can be written as

$$\bar{\mathbf{R}} \equiv \left\{ \begin{array}{c} [\mathsf{D}^e]^{-1} : (\boldsymbol{\sigma}_{n+1} - \boldsymbol{\sigma}^{\mathrm{trial}}) + \Delta\gamma\, \boldsymbol{N}_{n+1} \\ H^{-1}\,(\kappa_{n+1} - \kappa_n) - \Delta\gamma \\ \Phi(\boldsymbol{\sigma}_{n+1}, \kappa_{n+1}) \end{array} \right\} = \left\{ \begin{array}{c} \mathbf{0} \\ 0 \\ 0 \end{array} \right\}, \tag{10.126}$$

where D^e here denotes the isotropic (plane stress) elasticity operator and the unknowns are $\boldsymbol{\sigma}_{n+1}$, κ_{n+1} and $\Delta\gamma$.

Note that, unlike previously described implementations such as those of the von Mises and even the orthotropic Hoffman model, the return-mapping equation system in the present case cannot be reduced to a single scalar equation.

Newton–Raphson iteration

As usual, the solution of equation (10.126) is undertaken by the Newton–Raphson iterative scheme. To do this, it is convenient to split the residual vector $\bar{\mathbf{R}}$ as

$$\bar{\mathbf{R}} = \begin{Bmatrix} \mathbf{R} \\ \Phi \end{Bmatrix}; \quad \mathbf{R} \equiv \begin{Bmatrix} [\mathsf{D}^e]^{-1} : (\boldsymbol{\sigma}_{n+1} - \boldsymbol{\sigma}^{\mathrm{trial}}) + \Delta\gamma\, \boldsymbol{N}_{n+1} \\ H^{-1}\,(\kappa_{n+1} - \kappa_n) - \Delta\gamma \end{Bmatrix}. \tag{10.127}$$

Accordingly, the typical k^{th} Newton iteration comprises the solution of the linear system

$$\begin{bmatrix} [\mathsf{D}^e]^{-1} + \Delta\gamma\, \partial \boldsymbol{N}/\partial\boldsymbol{\sigma} & 0 & \boldsymbol{N} \\ 0 & 1/H & -1 \\ \boldsymbol{N} & -1 & 0 \end{bmatrix}^{(k-1)} \begin{Bmatrix} \delta\boldsymbol{\sigma}^{(k)} \\ \delta\kappa^{(k)} \\ \delta\Delta\gamma^{(k)} \end{Bmatrix} = - \begin{Bmatrix} \mathbf{R}^{(k-1)} \\ \\ \Phi^{(k-1)} \end{Bmatrix} \tag{10.128}$$

for the iterative increments of $\boldsymbol{\sigma}_{n+1}$, κ_{n+1} and $\Delta\gamma$. Following (10.116), the flow vector derivative can be expressed as

$$\frac{\partial \boldsymbol{N}}{\partial \boldsymbol{\sigma}} = \frac{\partial^2 \Phi}{\partial \boldsymbol{\sigma}} = \frac{1}{2M} \left(\frac{f}{2}\right)^{\frac{1-M}{M}} \frac{\partial^2 f}{\partial \boldsymbol{\sigma}^2} + \frac{1-M}{4M^2} \left(\frac{f}{2}\right)^{\frac{1-2M}{M}} \frac{\partial f}{\partial \boldsymbol{\sigma}} \otimes \frac{\partial f}{\partial \boldsymbol{\sigma}}. \tag{10.129}$$

Straightforward manipulation of system (10.128) gives the following solution (iterative increments) in symbolic form:

$$\delta\Delta\gamma^{(k)} = \frac{\Phi^{(k-1)} - [\boldsymbol{N}^{(k-1)} \quad -1\,]\, \mathbf{A}^{(k-1)}\, \mathbf{R}^{(k-1)}}{[\boldsymbol{N}^{(k-1)} \quad -1\,]\, \mathbf{A}^{(k-1)} \begin{Bmatrix} \boldsymbol{N}^{(k-1)} \\ -1 \end{Bmatrix}} \tag{10.130}$$

and

$$\begin{Bmatrix} \delta\boldsymbol{\sigma}^{(k)} \\ \delta\kappa^{(k)} \end{Bmatrix} = -\mathbf{A}^{(k-1)} \left[\mathbf{R}^{(k-1)} + \delta\Delta\gamma^{(k)} \begin{Bmatrix} \boldsymbol{N}^{(k-1)} \\ -1 \end{Bmatrix} \right], \tag{10.131}$$

where we have defined

$$\mathbf{A} \equiv \begin{bmatrix} \left\{ [\mathsf{D}^e]^{-1} + \Delta\gamma\, \partial \boldsymbol{N}/\partial\boldsymbol{\sigma} \right\}^{-1} & 0 \\ 0 & H \end{bmatrix}. \tag{10.132}$$

With the above solution at hand, we update the Newton guess for the unknowns according to

$$\boldsymbol{\Sigma}_{n+1}^{(k)} = \boldsymbol{\Sigma}_{n+1}^{(k-1)} + \delta\boldsymbol{\Sigma}^{(k)}, \tag{10.133}$$

where we have used the notation

$$\boldsymbol{\Sigma}_{n+1}^{(k)} \equiv \begin{Bmatrix} \boldsymbol{\sigma}_{n+1}^{(k)} \\ \kappa_{n+1}^{(k)} \\ \Delta\gamma^{(k)} \end{Bmatrix}; \quad \delta\boldsymbol{\Sigma}^{(k)} \equiv \begin{Bmatrix} \delta\boldsymbol{\sigma}^{(k)} \\ \delta\kappa^{(k)} \\ \delta\Delta\gamma^{(k)} \end{Bmatrix}. \tag{10.134}$$

Line-search procedure

Dutko *et al.* (1993) observed that the convergence bowl of the above Newton–Raphson scheme can be dramatically reduced for larger values of material constant M. Such an ill-conditioned behaviour stems from the high curvature present in the Barlat–Lian model for large M in the neighbourhood of points in stress space corresponding to the corners of the Tresca yield surface. Under such conditions, small changes in stress on the yield surface result in large changes in flow vector direction, characterising a set of *stiff* evolution equations. To tackle the problem, Dutko *et al.* (1993) adopted a line-search procedure which has effectively stabilised the Newton–Raphson scheme for the range of strain increments expected to be present in practical finite element computations with values of constant M as high as 40. Line-search procedures are discussed in detail by Fletcher (1980) (see also Matthies and Strang 1979, and Crisfield 1991).

The line-search in the present case is activated whenever the rate of convergence of the Newton–Raphson iterations falls below a prescribed minimum; that is, if for a Newton iteration $k \geq 2$ and a prescribed tolerance ϵ, the relation

$$|\delta \boldsymbol{\Sigma}^{(k)} \cdot \bar{\mathbf{R}}^{(k)}| \geq \epsilon \, |\delta \boldsymbol{\Sigma}^{(k)} \cdot \bar{\mathbf{R}}^{(k-1)}| \tag{10.135}$$

is satisfied, then the line-search algorithm is carried out. The interested reader is referred to Dutko *et al.* (1993) for a complete description of the algorithm.

Consistent tangent operator

Again, an expression for the elastoplastic consistent tangent can be easily obtained by means of a specialisation of the general procedure of Section 7.4.4. Then, by differentiating the return-mapping system (10.126) with respect to its unknowns $\boldsymbol{\sigma}_{n+1}$, κ_{n+1} and $\Delta\gamma$ as well as to its input, $\boldsymbol{\varepsilon}^{e\,\mathrm{trial}} = [\mathsf{D}^e]^{-1} : \boldsymbol{\sigma}_{n+1}^{\mathrm{trial}}$, we obtain

$$\begin{bmatrix} [\mathsf{D}^e]^{-1} + \Delta\gamma\, \partial \boldsymbol{N}/\partial \boldsymbol{\sigma} & 0 & \boldsymbol{N} \\ 0 & 1/H & -1 \\ \boldsymbol{N} & -1 & 0 \end{bmatrix} \begin{Bmatrix} \mathrm{d}\boldsymbol{\sigma}_{n+1} \\ \mathrm{d}\kappa_{n+1} \\ \mathrm{d}\Delta\gamma \end{Bmatrix} = \begin{Bmatrix} \mathrm{d}\boldsymbol{\varepsilon}^{e\,\mathrm{trial}} \\ 0 \\ 0 \end{Bmatrix}. \tag{10.136}$$

Note that this differential relation has the same symbolic format as expression (7.141), obtained for the von Mises isotropically hardening model. Accordingly, the elastoplastic tangent for the Barlat–Lian model with implicit return mapping is a complete analogy to (7.148) and can be expressed as

$$\mathsf{D}^{ep} \equiv \frac{\partial \boldsymbol{\sigma}_{n+1}}{\partial \boldsymbol{\varepsilon}^{e\,\mathrm{trial}}} = \mathsf{P} - \frac{1}{\boldsymbol{N} : \mathsf{P} : \boldsymbol{N} + H} \, (\mathsf{P} : \boldsymbol{N}) \otimes (\mathsf{P} : \boldsymbol{N}), \tag{10.137}$$

where

$$\mathsf{P} \equiv \left(\mathsf{I}_S + \Delta\gamma\, \mathsf{D}^e : \frac{\partial \boldsymbol{N}}{\partial \boldsymbol{\sigma}} \right)^{-1} : \mathsf{D}^e. \tag{10.138}$$

As a result of the associative nature of the plastic flow rule and hardening law (refer to Section 7.4.6, page 243), the above operator is symmetric.